



# 1 The CMIP6-downscaled CORDEX-Southeast Asia (SEA) ensemble: 2 evaluation and benchmarking for megacities of SEA

3 Phuong Loan Nguyen<sup>1,2</sup>, Lisa V. Alexander<sup>1,3</sup>, Thanh Ngo-Duc<sup>4</sup>, Faye Cruz<sup>5</sup>, Jerasorn Santisirisomboon<sup>6</sup>,  
4 Liew Juneng<sup>7</sup>, Donadi S. Permana<sup>8</sup>, Jing Xiang Chung<sup>9</sup>, Julie Mae Dado<sup>5</sup>, John L. McGregor<sup>10</sup>, Grace  
5 Redmond<sup>11</sup>, Tse Wai Po<sup>12</sup>, Fredolin Tangang<sup>7,13</sup>, Tan Phan-Van<sup>14</sup>, Son C. H. Truong<sup>10</sup>, Marcus  
6 Thatcher<sup>10</sup>, Long Trinh-Tuan<sup>15</sup>, Ummu Ma'rifah<sup>8</sup>, Jennifer Tibay<sup>5</sup>, Giovanni Di Virgilio<sup>1,2</sup>, Stephen  
7 White<sup>2</sup>

8 <sup>1</sup> Climate Change Research Centre, UNSW Sydney, New South Wales, Australia

9 <sup>2</sup> Climate & Atmospheric Science, NSW Department of Climate Change, Energy, the Environment and Water, New South  
10 Wales, Australia

11 <sup>3</sup> ARC Centre of Excellence for the Weather of the 21st Century, UNSW Sydney, New South Wales, Australia

12 <sup>4</sup> Department of Space and Earth Sciences, University of Science and Technology of Hanoi, Vietnam Academy of Science and  
13 Technology, Hanoi, Vietnam

14 <sup>5</sup> Manila Observatory, Ateneo de Manila University campus, Quezon City, Philippines

15 <sup>6</sup> Ramkhamhaeng University Center of Regional Climate Change and Renewable Energy (RU-CORE)

16 <sup>7</sup> Department of Earth and Environmental Sciences, Faculty of Science and Technology, University Kebangsaan Malaysia,  
17 Bangi, Selangor, Malaysia

18 <sup>8</sup> Indonesia Agency of Meteorology, Climatology, and Geophysics (BMKG), Jakarta, Indonesia

19 <sup>9</sup> Faculty of Science and Marine Environment, University Malaysia Terengganu, Kuala Nerus, Terengganu, Malaysia

20 <sup>10</sup> The Commonwealth Scientific and Industrial Research Organisation, Victoria, Australia

21 <sup>11</sup> Met Office Hadley Centre, Exeter, United Kingdom (UK)

22 <sup>12</sup> Hong Kong Observatory, Hong Kong

23 <sup>13</sup> Faculty of Arts and Social Sciences, University Brunei Darussalam, Brunei Darussalam

24 <sup>14</sup> Faculty of Meteorology, Hydrology, and Oceanography, University of Science, Vietnam National University

25 <sup>15</sup> Vietnam Academy for Water Resources (VAWR), Hanoi, Vietnam

26 Correspondence to: Phuong Loan Nguyen (loan.nguyen@dceew.nsw.gov.au)

27 **Abstract.** A 21-member ensemble of regional climate simulations has been produced for Southeast Asia (SEA) by dynamically  
28 downscaling Coupled Model Intercomparison Project Phase 6 (CMIP6) Global Climate Models (GCMs) under the World  
29 Climate Research Programme's Coordinated Regional Climate Downscaling Experiment (CORDEX). The ensemble was  
30 generated by several modelling institutes using three regional climate models (RCMs) with eight distinct model configurations,  
31 resulting in a total of 62 simulations spanning the historical period and multiple future emissions scenarios. Model performance  
32 for mean, daily maximum/minimum temperature, and precipitation was evaluated against multiple observations at annual,  
33 seasonal, and daily time scales over SEA and its two subregions: Mainland and Maritime Continent (MC). Despite large  
34 observational uncertainties in precipitation intensity, the CMIP6 CORDEX-SEA ensemble captures the spatial and seasonal



35 rainfall distribution reasonably well but tends to substantially overestimate observed rainfall. Wet biases, evident in about two-  
36 thirds of the models, are regionally and seasonally heterogeneous and larger over monsoon-dominated regions and seasons  
37 (e.g., MC during November–April and the Mainland during May–October). All RCMs showed widespread, statistically  
38 significant cold biases in daily mean temperature, which were largest during boreal winter, over the Mainland, and in  
39 simulations that have significant wet biases. These cold biases primarily arise from the models’ underestimation of daily  
40 maximum temperature. The MC remains a challenging region since models struggle to accurately capture the spatial variability  
41 of rainfall and the internal variability of temperature. A standardised benchmarking framework was applied to precipitation  
42 and temperature, which ultimately identified 15 historical simulations that met our a priori model performance expectations.  
43 Analysing the range of future projections and model independence shows that simulations from the same RCM family exhibit  
44 similar bias structures, highlighting the importance of RCM setup and the selection of statistically independent models. From  
45 this process, eight simulations spanning three RCM configurations were selected for further kilometre-scale dynamical  
46 downscaling over megacities of SEA.

## 47 **1 Introduction**

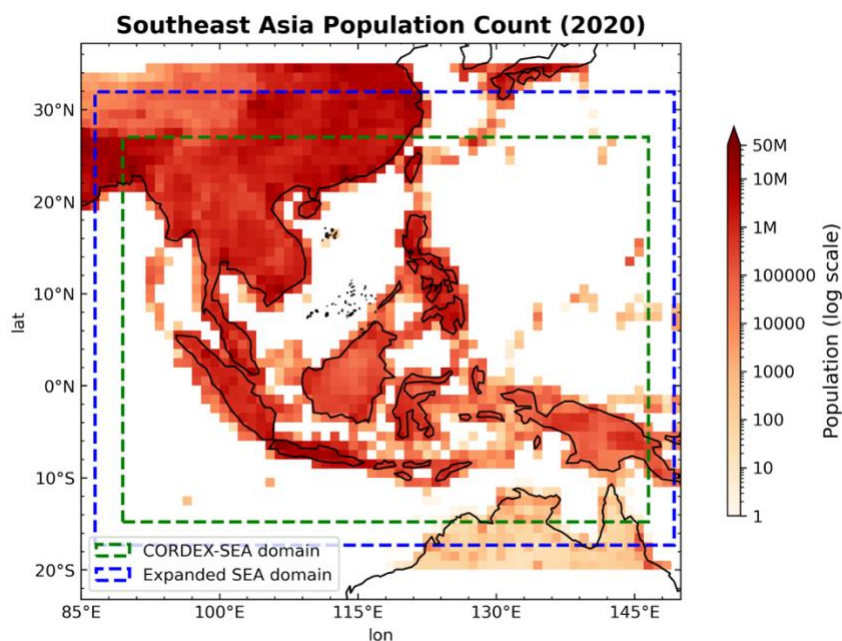
48 Despite climate change being a global phenomenon, its impacts vary significantly across regions. Current global climate  
49 models (GCMs) operated at a coarse spatial resolution (~100 - 250 km) limit their ability for direct use in many regional  
50 climate impact applications and contexts. GCMs often struggle to simulate sub-grid weather (e.g., local land use, complex  
51 topography, etc.) and therefore cannot accurately mesoscale local-scale processes and feedbacks (e.g., deep convection, land–  
52 atmosphere interactions, etc.) (Douville et al., 2021; Maraun and Widmann, 2018). As a result, climate information at finer  
53 scales (e.g., 50–4 km), from sub-continental to local, is essential for assessing impacts and risks (Doblas-Reyes et al., 2021;  
54 IPCC, 2021). To produce this information, regional climate modelling groups have been downscaling GCMs targeting specific  
55 regions under the World Climate Research Programme’s (WCRP) Coordinated Regional Climate Downscaling Experiment  
56 (CORDEX) initiatives (Giorgi et al., 2008; Giorgi and Gutowski, 2016).

57 Since its launch in 2009, CORDEX has facilitated the generation of regional climate simulations across 14 continental-scale  
58 domains, in parallel with the development of the Coupled Model Intercomparison Project (CMIP) phases (e.g., CORDEX-  
59 CMIP5). In addition, the CORDEX Coordinated Output for Regional Evaluation (CORDEX-CORE) has provided a  
60 homogenous set of projections for all CORDEX domains using three global climate models (GCMs) from CMIP5 (Giorgi et  
61 al., 2021). Along with the latest results presented in the Intergovernmental Panel on Climate Change (IPCC) Sixth Assessment  
62 Report (AR6) (IPCC, 2021), CMIP Phase 6 GCMs integrated with the Shared Socioeconomic Pathways (SSPs) (O’Neill et al.,  
63 2016) were introduced. In 2021, the experimental design for dynamical downscaling of CMIP6 models under CORDEX was



64 published (CORDEX, 2021), and modelling groups worldwide have since contributed simulations that provide well-grounded  
65 climate information for regional climate resilience and adaptation planning.

66 Southeast Asia (SEA), a home to more than 700 million people, is one of the key domains within the CORDEX framework  
67 (Fig. 1). The Southeast Asia Regional Climate Downscaling (SEACLID)/CORDEX-SEA project, launched in November 2013,  
68 represents the most comprehensive regional climate modelling initiative for this region, aiming to provide high-resolution  
69 climate information to support mitigation and adaptation planning. In its first phase, fourteen dynamical downscaling  
70 experiments at 25-km resolution were conducted over the domain (89.5°E–146.5°E, 14.8°S–27°N, Fig. 1) through  
71 collaboration among seven modelling centres worldwide (Tangang et al., 2020). The WCRP CORDEX-CORE initiative later  
72 contributed three additional CMIP5-driven simulations for the SEA domain. Overall, CMIP5 CORDEX-SEA simulations  
73 exhibit reasonable agreement with observations but often display systematic wet biases associated with specific regional  
74 models (Tangang et al., 2020). The multi-model ensemble (MME) of CMIP5 CORDEX-SEA generally provides an improved  
75 representation of climatological precipitation but also exhibits larger inter-model variability compared with MME GCMs.  
76 However, Nguyen et al. (2022) demonstrated that these regional climate models (RCMs) are not necessarily closer to the  
77 observed precipitation distribution than their driving GCMs. Following the CMIP6 CORDEX guidance, several modelling  
78 centres from SEA, Hong Kong, Australia, and the United Kingdom have recently initiated new downscaling experiments using  
79 CMIP6 GCMs for an expanded CORDEX-SEA domain (17.3°S–31.9°N, 86.5°E–149.3°E; Fig. 1), which now also fully spans  
80 Myanmar. This coordinated effort establishes a valuable foundation for generating updated regional climate projections (Table  
81 1). A necessary condition for projecting future regional climate is that a model can adequately simulate the observed climate,  
82 including the more extreme events that threaten vulnerable natural and socioeconomic systems. To facilitate the effective use  
83 of dynamically downscaled datasets in climate impact studies, we present here the first comprehensive cross-ensemble  
84 evaluation of CMIP6 CORDEX-SEA simulations in reproducing the observed and present-day climate characteristics.



85  
86  
87  
88  
89

**Figure 1. Southeast Asia's population in 2020, derived from the Gridded Population of the World (GPW), version 4, revision 11, provided by the Socioeconomic Data and Applications Center (SEDAC, 2018). The green dashed line indicates the CMIP5-downscaled CORDEX-SEA domain (89.5°E–146.5°E, 14.8°S–27°N), while the blue dashed line shows the expanded domain (86.5°E–149.3°E, 17.3°S–31.9°N) used for most CMIP6-downscaled simulations.**

90 Cross-ensemble evaluations of model ensembles over SEA have been conducted using various approaches. The most common  
91 method, often applied by research groups targeting specific applications. For example, models are ranked based on their ability  
92 to reproduce key climatological variables such as near-surface temperature and precipitation. This approach uses a set of  
93 statistical skill metrics, providing added value information of RCMs compared to their forcing GCMs (Tangang et al., 2020;  
94 Cruz et al., 2017; Juneng et al., 2016; Ngo-Duc et al., 2017; Nguyen et al., 2022), supporting the selection of suitable CMIP6  
95 GCMs (Desmet and Ngo-Duc, 2022) or the optimization of RegCM4 configurations (Ngo-Duc et al., 2024) for downscaling  
96 activities within the CORDEX-SEA domain. However, the results vary considerably across studies due to differences in the  
97 model ensembles and performance metrics employed. Consequently, a consistent observational benchmark and standardized  
98 evaluation framework are required to ensure comparability and robustness of assessments. Nguyen et al. (2024) implemented  
99 a standardized benchmarking framework [BMF; Ispording et al. (2024)] to evaluate CMIP6 models against multiple  
100 observational datasets, aiming to identify a “fit-for-purpose” subset of GCMs for dynamical downscaling applications over  
101 Southeast Asia. Model selection within this framework follows a two-step process: first, models must meet minimum  
102 performance thresholds in reproducing key climatological characteristics of temperature and precipitation; and second, they  
103 are assessed for their ability to capture dominant precipitation drivers (e.g., the monsoon system) and teleconnections with



104 major climate modes such as the Indian Ocean Dipole (IOD) and El Niño–Southern Oscillation (ENSO). The adoption of this  
105 standardised benchmarking approach represents a significant advancement, offering a transparent and objective foundation for  
106 model evaluation and strengthening confidence in future regional climate projections (Jiang et al., 2025).

107 Climate extremes such as heatwaves, flooding, and drought have already caused substantial economic losses and damages,  
108 particularly in rapidly growing megacities such as Bangkok, Hanoi, Jakarta, Kuala Lumpur, and Manila (IPCC, 2022).  
109 Projections indicate that some climate extremes in SEA will become more frequent and intense with additional global warming  
110 (Tangang et al., 2020; Seneviratne et al., 2021). As urbanization accelerates, it is critical that the development of these cities  
111 be guided by robust climate information to enhance resilience against future climate hazards. To address this need, the Climatic  
112 Hazard Assessment to Enhance Resilience against Climate Extremes for Southeast Asian Megacities (“CARE for SEA  
113 Megacities”) project was established under the SEACLID/CORDEX-SEA framework with support from the Asia-Pacific  
114 Network for Global Change Research (APN, 2023). The CARE for SEA Megacities project aims to generate city-scale climate  
115 hazard information for these five SEA megacities under multiple SSPs by further dynamically downscaling RCM outputs to  
116 kilometre-scale resolution. Given the computational expense of such high-resolution experiments, it is essential to select a  
117 subset of RCMs based on the cross-ensemble and fit-for-purpose evaluations described above, ensuring that projections are  
118 both robust and actionable for urban resilience planning.

119 This paper documents the experimental design for producing the updated CMIP6 dynamical downscaled climate projection  
120 over SEA, presents the first assessment of CMIP6 CORDEX-SEA simulations, and serves as a standard reference for  
121 CORDEX simulations over Southeast Asia. We assess GCM-driven historical simulations against multiple observational  
122 datasets, providing a quantitative evaluation of how well each GCM–RCM combination reproduces maximum, mean, and  
123 minimum temperature as well as precipitation. The evaluation is conducted across daily, monthly, and seasonal timescales for  
124 the entire SEA region and its two sub-regions: the Mainland and the Maritime Continent (MC). Furthermore, we benchmark  
125 precipitation and near-surface temperature from CMIP6 CORDEX-SEA ensembles using the BMF developed by Isphording  
126 et al. (2024) for subsetting models that can be considered for further kilometre-scale downscaling over the SEA megacities  
127 under the CARE for SEA Megacities project. In addition to applying the BMF, we also consider other factors, including model  
128 dependence and spread in future response, given the fact that a balanced selection of models across the different model  
129 “families” and spanning a reasonable range of future projections is desirable (Brunner et al., 2020; Di Virgilio et al., 2022;  
130 Nguyen et al., 2024; Grose et al., 2023; Sobolowski et al., 2025).

131 The remainder of this paper is structured as follows. Section 2 describes the RCM experimental design and analytical approach,  
132 considering observational uncertainties. Section 3 presents the model evaluation and results of the benchmarking framework  
133 to select a subset of RCMs for our purpose. Section 4 discusses the overall findings and concludes the paper.



134 **2. Methods**

135 **2.1 Models and Experiment Design**

136 This section documents the experiment design of the CMIP6 dynamically downscaled climate projection over SEA. Table 1  
137 lists the 62 CMIP6-downscaled simulations generated within the CORDEX-SEA framework available at the time of this  
138 analysis. These comprise three regional climate models (RCMs), eight model configurations, and eleven driving CMIP6 GCMs  
139 running across historical and future scenarios. A detailed description of the model configurations is provided in Table 2. The  
140 subset of GCMs was selected either based on their performance in reproducing key climatological features (Desmet and Ngo-  
141 Duc, 2022) or their ability to simulate dominant precipitation drivers (e.g., the monsoon) and teleconnections with major  
142 climate modes (e.g., IOD, ENSO), while considering model independence and the spread of future projections (Nguyen et al.,  
143 2024).

144 Most simulations cover the extended SEA domain (17.3°S–31.9°N, 86.5°E–149.3°E), which fully covers Myanmar, except  
145 for the CCAM-2021 simulations that span a slightly smaller region (14.8°S–27°N, 89.5°E–146.5°E). Simulation periods vary  
146 slightly across models but generally extend from 1960 to 2099, following the CMIP6 CORDEX Experiment Guidance  
147 (CORDEX, 2021), and include both SSP1-2.6 and SSP3-7.0 scenarios.

148 Eight RCM configurations are utilized in this study (Table 2). Non-hydrostatic RegCM [RegCM4-NH, Coppola et al. (2021)]  
149 simulations were conducted by several modelling institutions in SEA. Among the 44 physical parameterization combinations  
150 conducted using RegCM4-NH in the sensitivity analysis phase with ERA5 forcing, two configurations—EXP16 and EXP28—  
151 were selected based on their performance in reproducing near-surface temperature and precipitation (Ngo-Duc et al., 2024).  
152 Both use the University of Washington (UW) PBL scheme (Bretherton et al., 2004), but differ in their convective  
153 parameterizations: EXP16 employs the Tiedtke scheme (Tiedtke, 1989), while EXP28 uses the Kain–Fritsch scheme (Kain,  
154 2004). Resolved-scale precipitation is represented using the SUBEX scheme (Pal et al., 2000). Other parameterizations follow  
155 the default RegCM4-NH setup, including the Community Climate Model version 3 (CCM3) radiative transfer scheme (Kiehl  
156 et al., 1998), the Community Land Surface Model version 4.5 [CLM4.5; Lawrence et al. (2019)] and the Zeng ocean flux  
157 scheme with roughness option 1 (Zeng et al., 1998). Recently, RegCM version 5 (RegCM5) has been released, featuring a new  
158 non-hydrostatic dynamical core derived from the MOLOCH weather prediction model (Giorgi et al., 2023). Accordingly, two  
159 additional experiments were performed using this configuration.

160 The Conformal Cubic Atmospheric Model (CCAM) is a global stretched-grid atmospheric model developed by the  
161 Commonwealth Scientific and Industrial Research Organisation (CSIRO), in which the target region is simulated at higher  
162 resolution (McGregor, 2005; McGregor and Dix, 2008; Nguyen et al., 2012; McGregor, 2015; Katzfey et al., 2016; Truong  
163 et al., 2025). CCAM employs a non-hydrostatic semi-Lagrangian dynamical core with multiple physical parameterization



164 options (Truong and Thatcher, 2025). Three CCAM configurations were applied by two institutions: the Climate Change  
165 Research Centre at the University of New South Wales (UNSW-CCRC) and CSIRO Australia.

166 The UNSW-CCRC CCAM configuration uses a C192 stretched grid, providing 25 km resolution over Southeast Asia. It  
167 employs 54 vertical atmospheric levels (from 20 m to 40 km) and 40 oceanic levels (to 5 km depth). Spectral nudging (Thatcher  
168 and McGregor, 2009; Truong et al., 2026) is applied to large-scale wind, temperature, and surface pressure fields from the host  
169 GCMs (e.g., ACCESS-CM2 and EC-Earth3-Veg) at a 6-hourly frequency and scales of ~3000 km, beginning around 850 hPa  
170 (~1.5 km above the surface). The UNSW-CCRC CCAM 2017 and 2021 versions differ in their convective and planetary  
171 boundary layer (PBL) schemes: the 2017 version uses a prognostic Turbulent Kinetic Energy (TKE)-based PBL scheme  
172 (Hurley, 2007), whereas the 2021 version applies a diagnostic Richardson-number-based scheme and an updated mass-flux  
173 convective closure including downdraft, entrainment, and detrainment processes (McGregor, 2003).

174 The CSIRO-CCAM configuration follows an AMIP-style setup driven by bias- and variance-corrected sea-surface temperature  
175 (SST) and sea-ice fields from CMIP6 GCMs (Hoffmann et al., 2016). It employs a C96 stretched grid and a modified version  
176 of the 2021 convective scheme (Mod2021), with 27 vertical levels extending from 20 m to 40 km.

177 Both UNSW-CCRC and CSIRO-CCAM share similar subsystems for the ocean and land surface [e.g., the Community  
178 Atmosphere Biosphere Land Exchange System—CABLE; Kowalczyk et al. (2006)] and a prognostic aerosol scheme  
179 implemented within the Simplified Edwards-Slingo four-band (SE4) (Freidenreich and Ramaswamy, 1999; Schwarzkopf and  
180 Ramaswamy, 1999) radiation scheme based on CSIRO-Mk3.6 aerosols.

181 The UK Met Office RCM HadREM3-GA7.05 (Tucker et al., 2022) is a limited-area configuration of the global GA7.05 model  
182 (Walters et al., 2019) with some modifications described in Buonomo et al. (2024). The RCM has a grid with  $0.11^\circ \times 0.11^\circ$   
183 horizontal resolution (~12 km), a 4 minute timestep, and 63 levels (with an upper lid at ~39 km). It is driven at its lateral  
184 boundaries using a one-way nesting approach every 6 hours using variables from the driving GCMs (UKESM1-0-LL, EC-  
185 Earth3-Veg and NorESM2-MM). The RCM adjusts to the surface and lateral boundary forcing across a 13-point external rim.  
186 No nudging or parameter perturbations were used in either model configuration.

187 In HadREM3-GA7.05, convection is parameterized using a mass-flux approach based on Gregory and Rowntree (1990). Large  
188 scale microphysics is a single-moment scheme derived from that of Wilson and Ballard (1999), and large-scale cloud is based  
189 on the prognostic cloud fraction and prognostic condensate PC2 scheme. The land surface model used is the Joint UK Land  
190 Environment Simulator (JULES) (Best et al., 2011; Clark et al., 2011). Aerosol radiation and cloud effects are derived from  
191 the MACv2-SP data set for the historical (Stevens et al., 2017) and SSP3-7.0 (O'Neill et al., 2016) scenarios. Monthly 3D  
192 fields of shortwave and longwave optical properties (absorption, extinction, scattering, and asymmetry) and cloud droplet



193 number concentration on the 12 km model grid were calculated, and then these were prescribed as a time series in the RCM  
 194 simulation for use in its calculation of time-varying radiative forcing.

195 **Table 1. List of simulations carried out in CORDEX-SEA at the time of analysis (as of September 2025)**

No	RCM	Simulations					RCM (Institution contribution)
		Historical	SSP1-2.6	SSP2-4.5	SSP3-7.0	SSP5-8.5	
1	CCAM-2017-ACCESS-CM2	x	x		x		CCAM-2017 (UNSW-CCRC, Australia)
2	CCAM-2017-EC-Earth3-Veg	x	x		x		
3	CCAM-2021-ACCESS-CM2	x	x		x		CCAM-2021 (UNSW-CCRC, Australia)
4	CCAM-2021-EC-Earth3-Veg	x	x		x		
5	CCAM-Mod2021-ACCESS-CM2	x					CCAM-Mod2021 (CSIRO, Australia)
6	CCAM-Mod2021-GFDL-CM4	x					
7	HadGEM3-RA7-EC-Earth3-Veg	x			x		HadGEM3-RA7 (Met Office, UK)
8	HadGEM3-RA7-NorESM2-MM	x			x		
9	HadGEM3-RA7-UKESM1-0-LL	x			x		
10	RegCM-CESM2	x	x		x		RegCM4 (Manila Observatory, Philippines and USTH, Vietnam)
11	RegCM-CNRM-ESM2-1	x	x	x	x	x	RegCM4 (USTH, Vietnam)
12	RegCM-CNRM-ESM2-1-exp16	x	x	x	x		
13	RegCM-NorESM2-MM	x	x	x	x	x	
14	RegCM-CanESM5	x			x		RegCM4 (UKM, Malaysia)
15	RegCM-EC-Earth3-Veg	x			x		
16	RegCM-MPI-ESM1-2-HR	x			x		
17	RegCM-MIROC-ES2L	x	x	x	x	x	RegCM4 (BMKG, Indonesia)
18	RegCM-MIROC6-exp16v5	x		x		x	RegCM4 and RegCM5 (Thailand)
19	RegCM-CMCC-ESM2	x		x		x	
20	RegCM-EC-Earth3-Veg-exp28v5	x		x		x	
21	RegCM-NorESM2-MM-exp16	x	x	x	x	x	RegCM4 (HKUST, Hong Kong)

196



Table 2. Description of participating regional climate models

RCM	Planetary boundary layer physics	Cumulus physics	Radiation scheme	Land surface	Cloud microphysics schemes	Vertical Level	Nudging
CCAM-2017	Turbulent Kinetic Energy (TKE) (Hurley, 2007) closure scheme.	Updated version of mass-flux closure (McGregor, 2003) version 2017	Simplified Edwards-Slingo 4-band radiation scheme (more spectral bands for SW and LW) (SE4) (Freidenreich and Ramaswamy, 1999; Schwarzkopf and Ramaswamy, 1999)	CABLE land surface model (Kowalczyk et al., 2006)	a full mixed-phase, multi-category bulk microphysics scheme including liquid, ice, rain, snow, and graupel. (Rotstayn, 1997)	54	GCM nudging at 3000 km of u, v, t (Thatcher and McGregor, 2009)
CCAM-2021	Richardson-number based scheme (Ri)(McGregor, 1993)	Updated version of mass-flux closure (McGregor, 2003) version 2021					
CCAM-Mod42021	Richardson-number based scheme (Ri) (McGregor, 1993)	Updated version of mass-flux closure (McGregor, 2003), modified version 2021					
RegCM4-NH-exp16	University of Washington (UW) (Bretherton et al., 2004)	Tiedtke (Tiedtke, 1989)					
RegCM5-NH-exp16		Kain-Fritsch (KF) (Kain, 2004)					
RegCM4-NH-exp28							
RegCM5-NH-exp28							
HadGEM3-RA7	Wilson et al. (1999)	Mass-flux scheme (Gregory and Rowntree, 1990)	MACv2-SP (Stevens et al., 2017; O'Neill et al., 2016)	Joint UK Land Environment Simulator (JULES) (Best et al., 2011; Clark et al., 2011)	Prognostic cloud fraction and prognostic condensate PC2 scheme.	63	NA



199 **2.2 Observations and data**

200 **Table 3. List of observational datasets of precipitation and temperature used in this study. Datasets marked with an asterisk (\*)**  
 201 **include daily maximum and minimum temperature data, while those marked with a double asterisk (\*\*) include monthly data only.**

Variables	Name	Short name	Coverage		Resolution		References
			Temporal	Spatial	Temporal	Spatial (°)	
Precipitation	APHRODITE_MA V1101 and V1101 XR	APHRODITE	1951–2015	60°E–15°E 15°S–55°N	Daily	0.25 x 0.25	Yatagai et al. (2012)
	REGEN_ALL_2019	REGEN_ALL	1950–2016	90°S–90°N	Daily	1 x 1	Contractor et al. (2020)
	CHIRPS_v2.0	CHIRPS	1981–2023	50°S–50°N	Daily	0.05 x 0.05	Funk et al. (2015)
	GPCC_FDD_2022	GPCC_FDD	1982–2020	90°S–90°N	Daily	1 x 1	Ziese (2022)
	SACA&D	SACAD	1981–2017	20°S–25°N 80°E–180°E	Daily	0.25 x 0.25	Van Den Besselaar et al. (2017)
Temperature	APHRO_MA V1808	APHRODITE	1961–2015	60°E–150°E 15°S–55°N	Daily	0.25 x 0.25	Yasutomi et al. (2011)
	ERA5*	ERA5	1940–2024	90°S–90°N	Daily	0.25 x 0.25	Hersbach et al. (2020)
	BEST*	BEST	1960–2019	90°S–90°N	Daily	1 x 1	Rohde and Hausfather (2020)
	CRU TS v4.08**	CRU TS	1901–2014	90°S–90°N	Monthly	0.5 x 0.5	Harris et al. (2020)
	SACA&D*	SACAD	1981–2017	20°S–25°N 80°E–180°E	Daily	0.25 x 0.25	Van Den Besselaar et al. (2017)

202 In this research, the evaluation and benchmarking of the performance of the CMIP6 CORDEX-SEA ensemble in simulating  
 203 climate variables focuses on precipitation and temperature over land, as the temporal coverage of oceanic observational  
 204 products is limited. We use multiple global and regional gridded observational datasets to account for observational  
 205 uncertainties in model evaluation (Nguyen et al., 2020). The selected datasets are summarized in Table 3. Precipitation datasets  
 206 include Asian Precipitation-Highly-Resolved Observational Data Integration Towards Evaluation of water resources  
 207 (APHRODITE) (V1101 and V1101EX) at 0.25° resolution (Yatagai et al., 2012); Rainfall Estimates on a Gridded Network  
 208 with 1° × 1° resolution [REGEN version Allstns V1 2019 (Contractor et al., 2020) ] and Climate Hazards Group InfraRed  
 209 Precipitation with Station at 0.25° × 0.25° resolution [CHIRPS version 2.0 (Funk et al., 2015) ] They were chosen based on  
 210 their demonstrated consistency in capturing daily precipitation and extremes over SEA (Nguyen et al., 2020; Nguyen et al.,



211 2023). For daily near-surface temperature, we also use APHRODITE\_MA V1808 at 0.25° resolution (Yasutomi et al., 2011);  
212 Berkeley Earth Surface Temperatures [BEST; Rohde and Hausfather (2020)]; the Climate Research Unit (CRU) TS v4.08  
213 dataset at 0.5° resolution (Harris et al., 2020); and the ECMWF Reanalysis v5 (ERA5; Hersbach et al., 2020) at 0.25°  
214 resolution. Recognizing the sparse observational network over the Maritime Continent in both global datasets and the regional  
215 high-resolution dataset of APHRODITE (Yatagai et al., 2012), we additionally include the Southeast Asia Climate Assessment  
216 and Dataset (SACAD) version 2.0 at 0.25° resolution. Providing precipitation, mean, maximum, and minimum temperature at  
217 a daily scale, this dataset enhances the station network density and coverage, particularly over Indonesia, through contributions  
218 from the Indonesian meteorological institutes (Van Den Besselaar et al., 2017).

219 Hereafter, APHRODITE is selected as the primary baseline for all main precipitation figures, as it utilizes the largest number  
220 of rain gauges among global datasets and compensates for the limited spatial coverage of SACAD. Note that for temperature,  
221 APHRODITE and CRUTS do not provide maximum, minimum, and mean temperature data at a daily time scale, while  
222 SACAD has limited spatial coverage (Fig. S1). Therefore, BEST is chosen as the reference dataset because it is an  
223 observational dataset that provides daily mean, maximum, and minimum temperature data across our Southeast Asia domain  
224 (89.26°E–127.28°E, 15.14°S–27.26°N). It should also be noted that inhomogeneities in the raw observations are not fully  
225 corrected in the BEST algorithm, which may introduce systematic temperature biases (e.g., the underestimation of temperature  
226 trend and magnitude), as previously reported in Canada (Way et al., 2017). Results from all other observational datasets are  
227 included in the Supplement (Figures S2–S11), with detailed explanations provided within the main text for intercomparison  
228 purposes.

229 All simulations are analyzed over the climatological period 1982–2014, the overlapping coverage of multiple observations and  
230 simulations. For trend analysis, the period is extended to 1960–2014 to maximize the common period across all RCM  
231 simulations. Prior to assessment, all observational datasets and model outputs are regridded to the common 0.22° models' grid  
232 using conservative remapping for precipitation and bilinear interpolation for temperature for a fair comparison.

## 233 **2.3. Methodology**

### 234 **2.3.1 Model evaluation**

235 This section describes our approach to address the second objective of this study, which is to evaluate the ability of the CMIP6  
236 CORDEX-SEA ensemble in simulating climatology of four model core variables: mean, maximum and minimum temperature  
237 and precipitation. Note that SEA exhibits clear seasonal and spatial contrasts in precipitation distribution. In particular, high  
238 rainfall is observed over the Mainland and less precipitation over MC during May-October (MJJASO). Meanwhile, the  
239 Mainland receives less precipitation while MC receives more precipitation during November-April (NJDFMA) (Juneng et al.,



240 2016; Nguyen et al, 2022). Therefore, analyses of monthly totals of wet-day precipitation ( $\geq 1\text{mm}$ , *prcptot*) are conducted at  
241 the seasonal scale, focusing on two distinct seasons: NDJFMA and MJJASO. Meanwhile, annual and two seasonal means of  
242 the boreal winter (December-January-February, DJF) and summer (June-July-August; JJA) are calculated using daily data for  
243 mean, maximum, and minimum temperatures. Analysis is conducted for the whole SEA domain ( $89.26^{\circ}\text{E}$ – $147.28^{\circ}\text{E}$ ,  $15.14^{\circ}\text{S}$ –  
244  $27.26^{\circ}\text{N}$ ) and its two sub-regions: Mainland ( $5^{\circ}\text{N}$ – $27.5^{\circ}\text{N}$ ;  $89.26^{\circ}\text{E}$ – $147.28^{\circ}\text{E}$ ) and MC ( $15.14^{\circ}\text{S}$ – $5^{\circ}\text{N}$ ;  $89.26^{\circ}\text{E}$ – $147.28^{\circ}\text{E}$ ).  
245 The performance of each RCM in reproducing observed climate over these timescales is assessed using several metrics: (i)  
246 model bias, defined as the regionally averaged difference between simulated and observed values; (ii) mean absolute  
247 percentage error (MAPE); and (iii) spatial correlation with observations, which is adopted from the standardized benchmarking  
248 framework (Ispording et al., 2024). To assess the statistical significance of model biases, the Mann–Whitney U test ( $\alpha = 0.05$ )  
249 is applied for precipitation due to its non-normal distribution, while a student’s t-test assuming equal variance ( $\alpha = 0.05$ ) is  
250 applied for temperature.

251 The RCM’s ability to simulate observed climate variables at daily time scales was also assessed by comparing each quantile in  
252 the daily mean observational distribution with those of the RCMs through quantile-quantile (Q-Q) plots. Then the distributions  
253 of RCMs and observations are compared using the area score metric (Nguyen et al., 2022), which measures the areas created  
254 by RCMs and observational lines using the trapezoidal rule.

### 255 2.3.2 Benchmarking

256 This section details the methodology to meet the third objective of this study, which is to identify a subset of CMIP6-  
257 downscaled RCMs that meet predefined performance criteria so as to be considered for further high-resolution dynamical  
258 downscaling at kilometre-scale over SEA megacities as part of the “CARE for SEA megacities” project. Scientists from the  
259 CORDEX–SEA community, in consultation with local policymakers and stakeholders from each city, have identified priority  
260 hazards, which include heat and rainfall extremes ([https://cordex.org/wp-](https://cordex.org/wp-content/uploads/2024/01/CARE_for_SEA_megacities_workshop_summary.pdf)  
261 [content/uploads/2024/01/CARE\\_for\\_SEA\\_megacities\\_workshop\\_summary.pdf](https://cordex.org/wp-content/uploads/2024/01/CARE_for_SEA_megacities_workshop_summary.pdf)). This prioritization underscores the need for  
262 models that can accurately represent the seasonal and spatial variability of temperature and precipitation across SEA. In  
263 addition to performance, the final subset of selected models should maintain diversity and minimize redundancy, ensuring that  
264 the ensemble captures a broad range of plausible future outcomes while remaining relevant and useful for decision-making.

265 Therefore, model selection is conducted in three stages. First, we benchmark all RCMs against multiple observational datasets  
266 for precipitation and near-surface temperature to assess their ability to reproduce key climatological characteristics using  
267 minimum standard metrics (MSMs) from the standardized benchmarking framework proposed by Ispording et al. (2024) with  
268 several modifications and additional considerations. In particular, MSMs include (i) mean absolute percentage error (MAPE)



269 for precipitation and mean absolute error (MAE) for temperature; (ii) spatial correlation (Scor); (iii) seasonal cycle (Scyc); and  
270 (iv) significant temporal changes (Isphording et al., 2024). These metrics are designed to evaluate model skill in simulating  
271 the spatial and temporal variability, timing, and quantity of rainfall and temperature. In this research, we use multiple in situ  
272 and satellite-based observational datasets for evaluation. Figure S1 presents the spatial distribution of seasonal total  
273 precipitation and annual daily mean, maximum, and minimum temperature across multiple observational products. Given the  
274 substantial observational uncertainties associated with temperature and precipitation (Nguyen et al., 2020), assessment against  
275 a single reference dataset is not considered sufficient justification for model selection; instead, a model is excluded only if its  
276 skill scores exceed predefined thresholds for at least half (e.g., three out of five in this study) of the reference datasets.

277 In the second stage, we consider the projected CMIP6 CORDEX–SEA climate change signals for 2070–2099 relative to 1981–  
278 2010 during the MJJASO and NDJFMA seasons to ensure that the expected subset spans a range of plausible future outcomes.  
279 In the final stage, we examine inter-model dependencies using hierarchical clustering based on the historical climatology of  
280 temperature and precipitation, following Nguyen et al. (2024) and Gibson et al. (2024) This step ensures that at least two  
281 simulations are retained from each independent modelling group to minimize redundancy.

282 Note that due to the limited availability of reliable city-scale observational datasets, the benchmarking is conducted over the  
283 land of the entire SEA domain, rather than at city scale.

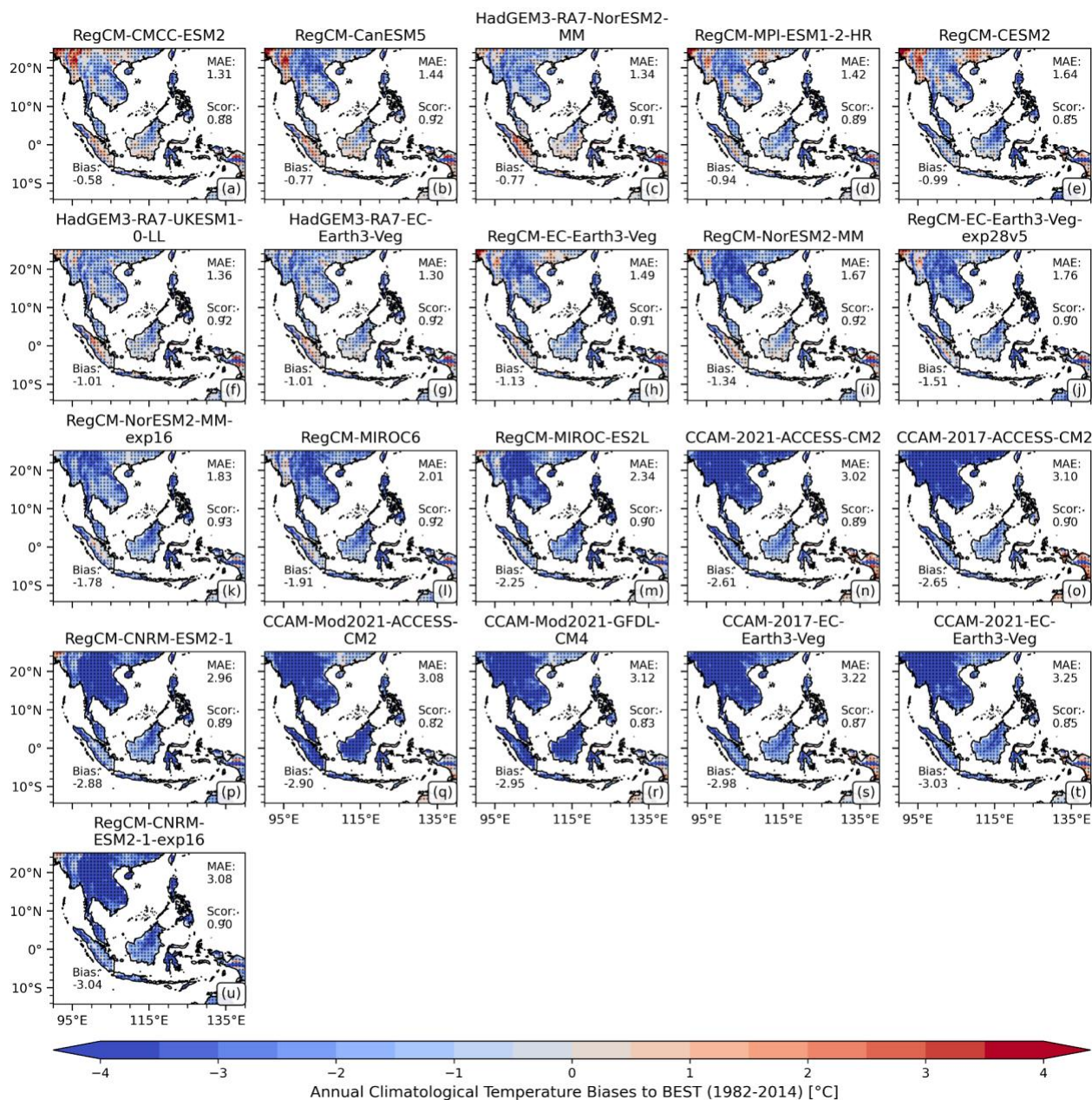
### 284 **3. Results**

#### 285 **3.1 Near-surface mean, maximum and minimum temperature**

286 We evaluated the performance of the CMIP6-driven CORDEX-SEA simulations by comparing simulated and observed annual  
287 mean daily temperature (*tas*) from BEST over 1982–2014 (Fig. 2). Overall, the simulations reproduce the spatial patterns of  
288 observed temperature reasonably well, with Pearson’s correlations (Scor) exceeding 0.8 in all cases. However, despite this  
289 consistency, all simulations systematically underestimate near-surface temperature. The area-averaged bias across terrestrial  
290 SEA ranges from  $-0.58^{\circ}\text{C}$  to  $-3.04^{\circ}\text{C}$ , which is substantially larger than the spread among reference datasets ( $-0.45^{\circ}\text{C}$  to  
291  $0.45^{\circ}\text{C}$ ; Fig. S1). Seasonally, the cold bias is more pronounced during boreal winter (DJF) than boreal summer (JJA) (Fig.  
292 S2a). Most RCMs show statistically significant cold biases between approximately  $-5^{\circ}\text{C}$  and  $-1.5^{\circ}\text{C}$  across most grid points  
293 of the domain. The spatial distribution of these biases is strongly dependent on the RCM rather than the driving GCM. For  
294 example, RegCM simulations show cold biases over the mainland and western Indonesia but warm biases over parts of  
295 northwestern Mainland SEA (e.g., Myanmar), whereas CCAM and HadGEM3-RA7 simulations exhibit widespread cold  
296 biases across nearly the entire region. CCAM simulations, in particular, stand out with substantial cold biases exceeding  $3^{\circ}\text{C}$ ,



297 likely linked to excessive simulated precipitation (see Section 3.4). It's note that some driving GCMs (e.g., EC-Earth3-Veg,  
298 NorESM2-MM, MPI-ESM1-2-HR) also exhibits a cold biases, although these are less pronounced (Nguyen et al., 2024),  
299 whereas others (e.g., CMCC-ESM2, ACCESS-CM2, UKESM1-0-LL) exhibits warm biases. These results suggest that  
300 systematic errors in daily mean temperature are strongly influenced by the RCM rather than by the driving GCMs. In terms of  
301 mean absolute errors (MAE) to observation, CCAM simulations tend to show the biggest errors compared with other  
302 simulations, with the biggest difference over the Mainland and during the boreal winter (DJF) (Fig. S3).



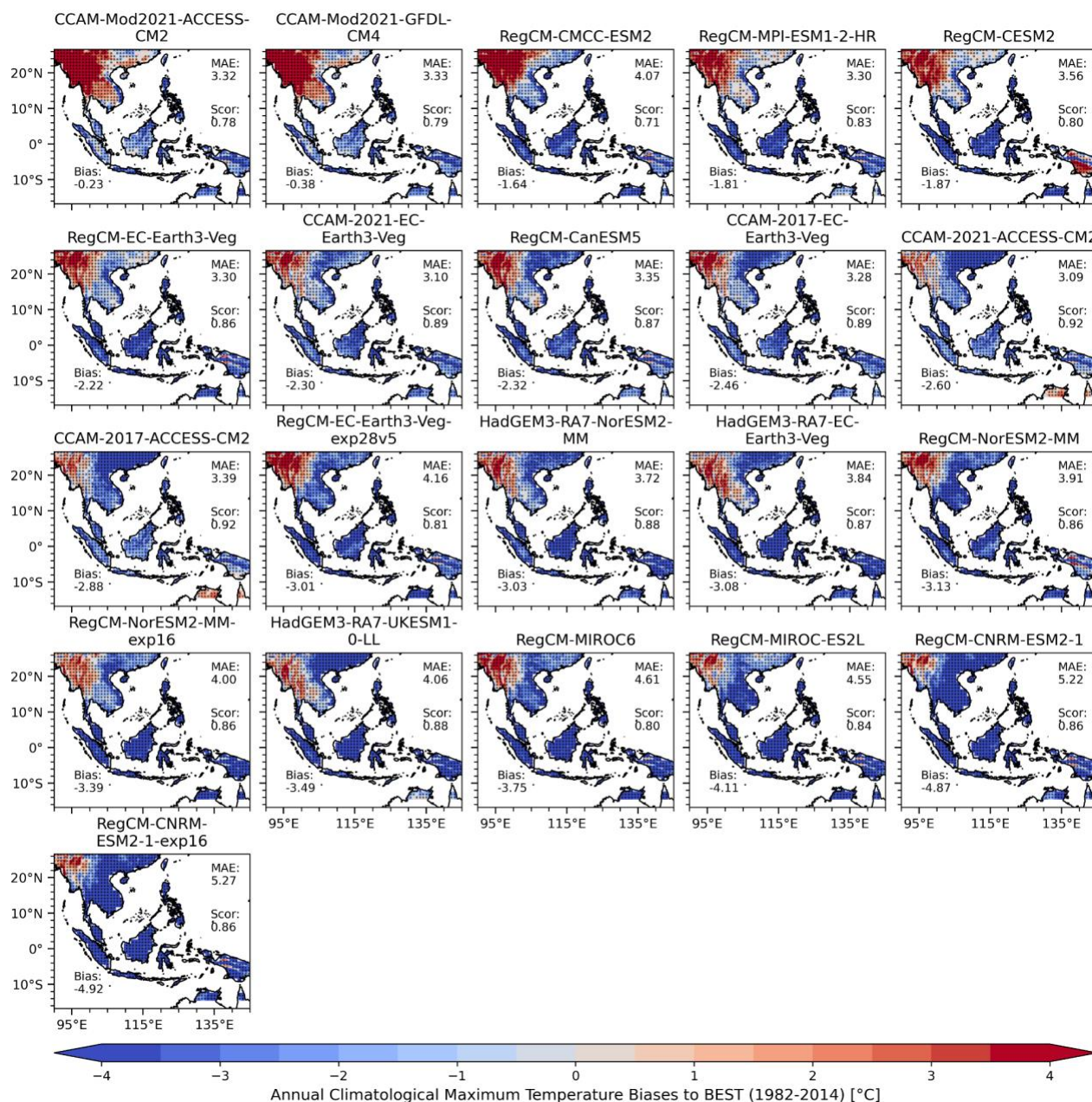
303

304 **Figure 2.** Annual climatological (1982–2014) mean near-surface temperature biases (in °C) for each model, ranked from warmest to  
 305 coolest based on regionally averaged bias, against observational product BEST. The mean absolute errors (MAEs) and spatial  
 306 correlations (Scor) calculated against BEST are shown in the upper-right corner. All analyses are considered at the resolution of the  
 307 CMIP6-downscaled CORDEX-SEA simulation (i.e., ~ 25 km). Stippled areas indicate locations where an RCM shows statistically  
 308 significant bias ( $p < 0.05$ ) according to the student t-test.



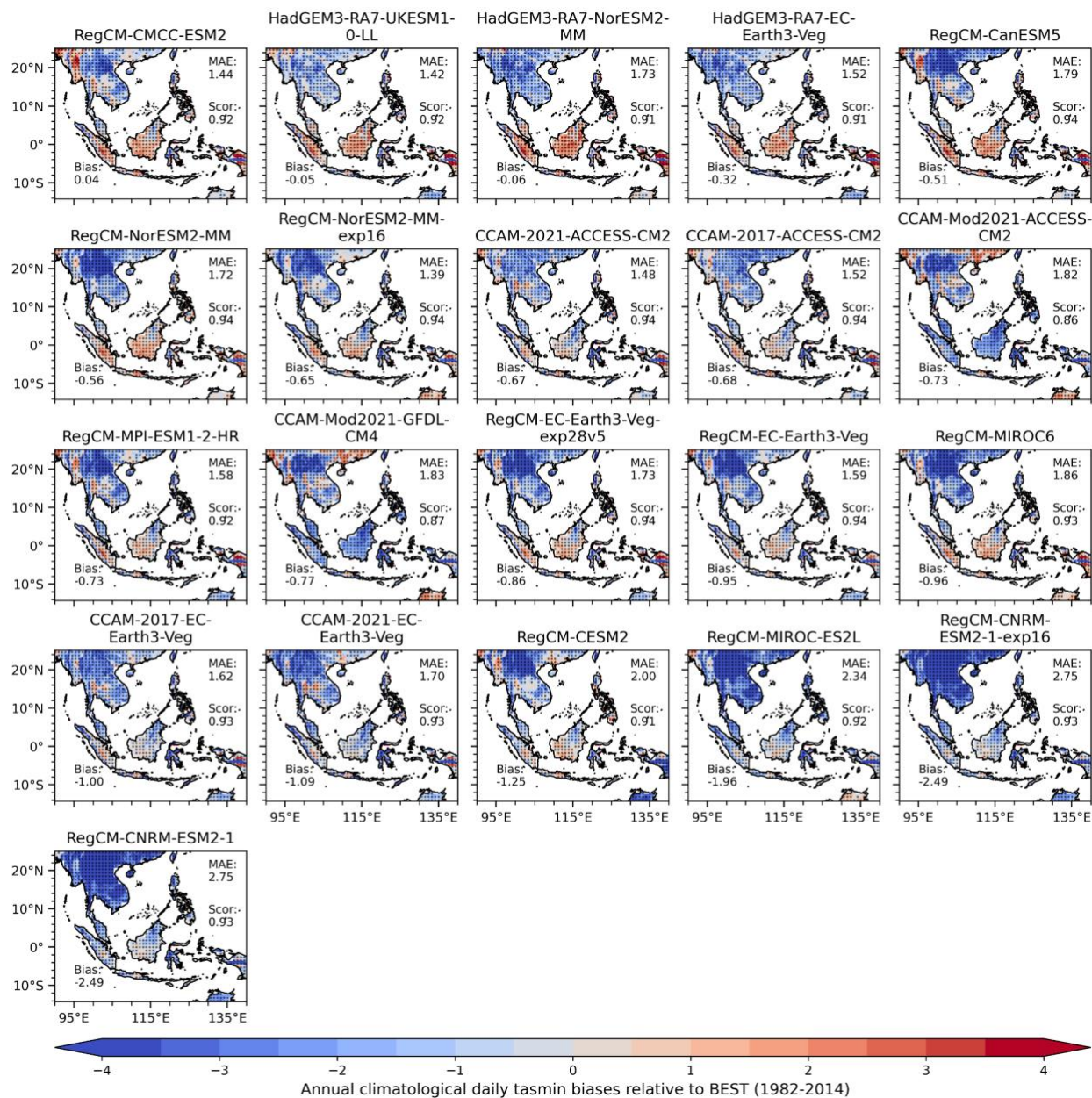
309 Figure S4 shows the seasonal cycle of near-surface temperature over two subregions: Mainland and MC, highlighting the  
310 systematic underestimation by CMIP6 CORDEX-SEA simulations. Overall, the RCMs capture the phase of the seasonal cycle  
311 well but tend to underestimate temperature magnitude throughout most months of the year, particularly during the boreal  
312 winter (DJF) over the Mainland. While most RCMs realistically simulate both the lower (DJF) and higher (MJJ) peaks over  
313 the Mainland (Fig. S4a), several simulations (e.g., RegCM4-MIROC6 and RegCM4-MIROC-ESM2L) fail to reproduce these  
314 features over MC (Fig. S4b). The mainland exhibits a clearly unimodal seasonal cycle, with a wide amplitude (e.g., 12–26°C)  
315 between lower and higher peaks, whereas the MC displays a bimodal cycle with a narrower range (e.g., 23–26.5°C).

316 To better understand the biases in mean temperature, we further examined model performance in daily maximum temperature  
317 (*tasmax*) and minimum temperature (*tasmin*) (Fig. 3 and Fig. 4, respectively). In general, the spatial coherence of RCMs (e.g.,  
318 Scor) with observations in *tasmax* is weaker than that for *tas*, although Scor values exceed 0.7 across models. In addition,  
319 many RCMs substantially underestimate *tasmax* both annually (Fig. 3) and seasonally (Fig. S5), where regionally averaged  
320 *tasmax* biases vary widely across simulations (e.g., ranging from -4.92°C to -0.38°C at the annual scale; Fig. 3). These are the  
321 major contributions to the cold biases in *tas* found in Fig. 1. Notably, there are significant differences between the Mainland  
322 and MC. In particular, while all RCMs show a significant cold bias over MC, most RCMs show a mix of warm biases over the  
323 northwest and cold biases over the remainder of the Mainland. Interestingly, simulations from the same RCM setup show very  
324 similar spatial biases but differ in magnitude. For example, CCAM-Mod2021 simulations exhibit considerable warm biases  
325 north of 15° N, while RegCM simulations show strong warm biases exceeding 4°C over Myanmar and pronounced cold biases  
326 over the MC. Further seasonal and sub-regional analyses reveal that *tasmax* cold biases intensify (Fig. S5) and expand spatially  
327 during boreal summer (figures not shown), whereas during winter these cold biases weaken, often disappearing or even  
328 reversing to warm biases over parts of the Mainland. Consistent with these patterns, MAE values for *tasmax* peak during boreal  
329 summer in most simulations (Fig. S6).



330

331 **Figure 3.** Annual climatological (1982–2014) daily maximum temperature biases (in °C) for each model, ranked from warmest to  
 332 coolest based on regionally averaged bias, against observational product BEST. The mean absolute error (MAE) and spatial  
 333 correlation (Scor) calculated against BEST are shown in the upper-right corner. All analyses are considered at the resolution of the  
 334 CMIP6-downscaled CORDEX-SEA simulation (i.e., ~ 25 km). Stippled areas indicate locations where an RCM shows statistically  
 335 significant bias ( $p < 0.05$ ) according to the student t-test.



336

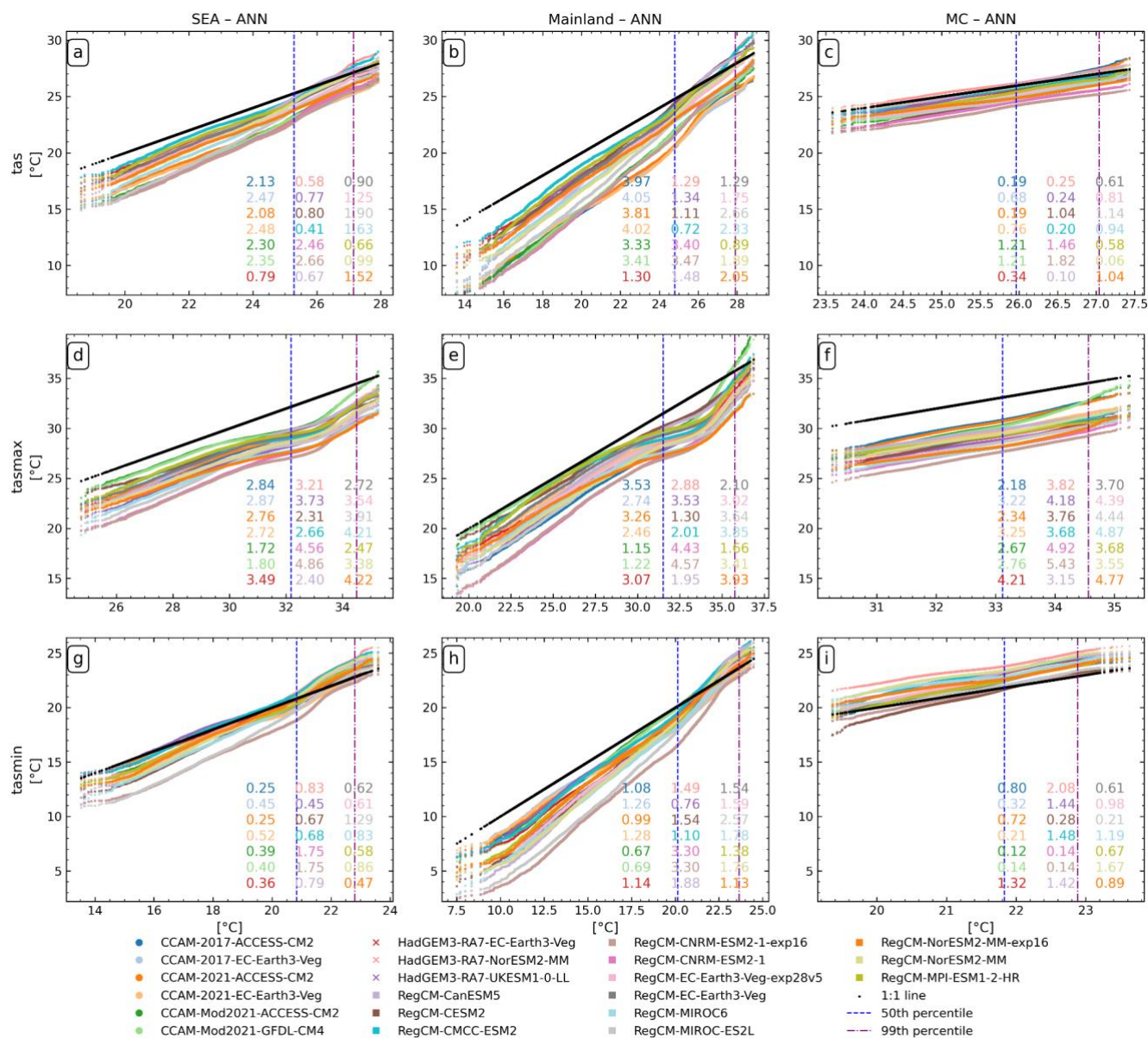
337 **Figure 4.** Annual climatological (1982–2014) daily minimum temperature biases (tasmin, in °C) for each model, ranked from  
 338 warmest to coolest based on regionally averaged bias, against observational product BEST. The mean absolute error (MAE) and  
 339 spatial correlation (Scor) calculated against BEST are shown in the upper-right corner. All analyses are considered at the resolution  
 340 of the CMIP6-downscaled CORDEX-SEA simulation (i.e., ~ 25 km). Stippled areas indicate locations where an RCM shows  
 341 statistically significant bias ( $p < 0.05$ ) according to the Student t-test.



342 In contrast, biases in daily minimum temperature (*tasmin*) are generally much smaller in magnitude but exhibit greater spatial  
343 heterogeneity across models and grid points than those in *tas* and *tasmax* (Fig. 4). CMIP6-downscaled simulations typically  
344 underestimate *tasmin* annually, with regionally averaged biases ranging from  $-0.04^{\circ}\text{C}$  to  $-2.52^{\circ}\text{C}$ . Spatially, cold biases in  
345 *tasmin* are more pronounced over the northern and eastern Mainland. Meanwhile, over the MC, the signal is more  
346 heterogeneous, with weaker cold biases or even warm biases in several simulations (e.g., HadGEM3-RA7, RegCM-CMCC-  
347 ESM, RegCM-CanESM5, and RegCM-NorESM2-MM). Seasonally, *tasmin* cold biases are generally stronger during DJF  
348 (Fig. S7), with MAE values also peaking in the boreal winter (DJF) for most simulations (Fig. S8). In contrast, during boreal  
349 summer (JJA), nearly half of the simulations (10 out of 22) exhibit warm biases in *tasmin* (Fig. S7).

350 The ability of the CMIP6-driven CORDEX-SEA simulations to reproduce the whole observed temperature distribution at the  
351 daily time scale was further evaluated using quantile–quantile (Q–Q) analysis and ASM (Sect. 2.3.1) (Fig. 5). The higher the  
352 ASM, the further away it is from the observations. ASM was calculated for the entire SEA domain in boreal summer and  
353 winter (Fig. S9 and S10, respectively) and for *tas*, *tasmax* and *tasmin*. To provide a detailed assessment across the full  
354 distribution, temperature was evaluated across three intervals: the lower half (0–50th percentile), the central-to-upper range  
355 (50–99th percentile), and the extreme upper tail (>99th percentile).

356 Consistent with the mean bias results, the Q–Q plots for daily mean temperature (*tas*, Fig. 5a–c) show that most RCM  
357 simulations lie below the observational reference line, confirming a systematic cold bias across much of the distribution. These  
358 discrepancies are most pronounced at the lower end of the distribution (below the 50th percentile), indicating that models  
359 particularly underestimate cooler-than-average conditions. This deficiency is strongest over Mainland SEA and during boreal  
360 winter (Fig. S10d–f), consistent with the seasonal and regional bias patterns identified earlier. In contrast, model performance  
361 improves at higher percentiles, where simulated temperatures are closer to observations, and in some cases even exceed  
362 observed values at the extreme upper tail (>99th percentile). Model skill varies substantially among simulations. For example,  
363 RegCM-CMCC-CESM2, HadGEM3-RA7-NorESM2-MM, and RegCM-MPI-ESM1-2-HR consistently rank among the best-  
364 performing simulations, with the lowest ASM values across regions and seasons. In contrast, RegCM-CNRM-ESM2-1-exp16  
365 and CCAM-Mod2021 simulations driven by ACCESS-CM2 and GFDL-CM4 exhibit the largest ASM values, reflecting  
366 pronounced cold biases and broader distributional errors (Fig. S3).



367

368 **Figure 5. Quantile-quantile plots for regionally averaged daily near-surface temperature (tas, in °C; a-c), maximum temperature**  
 369 **(tasmax; d-f), and minimum temperature (tasmin; g-i) across Southeast Asia and its two sub-regions: Mainland (5°N–27.5°N, 89°E–**  
 370 **147°E) and the Maritime Continent (15°S–5°N, 89°E–147°E) during the climatological period of 1982–2014. The inserted number**  
 371 **indicates the values of the area score metric (ASM; Nguyen et al., 2022), which measures the proximity between the two distributions:**  
 372 **the model and the reference (BEST) (section 2.3.1). The vertical lines indicate the 50<sup>th</sup> percentile (blue) and 99<sup>th</sup> percentile (purple),**  
 373 **respectively.**



374 These distributional biases in *tas* are closely linked to deficiencies in simulating *tasmax*, which shows larger and more  
375 systematic departures from observations (Fig. 5d-f). Most RCM simulations fall well below the observational reference line  
376 across much of the distribution over SEA and its two subregions, confirming widespread cold biases. These biases are  
377 particularly pronounced in the mid-range of the distribution (50th–90th percentiles, corresponding to approximately 32–34°C),  
378 indicating that models struggle to reproduce typical daytime temperature conditions. Interestingly, this deficiency is largely  
379 driven by errors over MC, whereas performance over the mainland is somewhat improved compared with that in the Mainland.  
380 Interestingly, CCAM-Mod2021 simulations exhibit distinct behavior in simulating the distribution of *tasmax*, with warm  
381 biases emerging at the extreme upper tail (>99th percentile), particularly over the Mainland. Among CMIP6-downscaled  
382 RCMs, CCAM-Mod2021-ACCESS-CM2 generally shows better agreement with observations than most other simulations.  
383 Meanwhile, RegCM-CNRM-ESM2-1-exp16 consistently ranks among the top five poorest-performing simulations based on  
384 ASM across both annual and seasonal timescales (Figs. S6, S9, and S10). More broadly, RegCM simulations tend to reproduce  
385 the *tasmax* distribution less accurately than other RCM families. These results highlight the earlier finding that cold biases in  
386 *tasmax* are a primary driver of errors in *tas* particularly due to the models' inability to accurately represent the central and  
387 upper portions of the temperature distribution.

388 In contrast, the RCMs generally demonstrate better skill in reproducing the distribution of *tasmin*, although systematic biases  
389 remain (Fig. 5g-i). Unlike *tas* and *tasmax*, *tasmin* biases exhibit a distinct pattern, with models tending to underestimate cooler-  
390 than-average conditions (below the 50th percentile) and overestimate warmer-than-average conditions (above the 50th  
391 percentile). This indicates an overall compression of the temperature distribution, with insufficient representation of the full  
392 observed variability. Despite this, several simulations (e.g., CCAM-Mod2021-ACCESS-CM2, CCAM-2017-ACCESS-  
393 CM2, CCAM-2017-EC-Earth3-Veg, and HadGEM3-RA7-EC-Earth3-Veg) show relatively good agreement with observations  
394 across the full distribution and across multiple reference datasets (Figs. S8-10). In contrast, some RegCM simulations,  
395 particularly RegCM-CNRM-ESM2-1 and RegCM-MIROC6, exhibit substantially poorer performance, with large ASM values  
396 reflecting systematic underestimation across much of the distribution, especially on annual and winter timescales.

397 Regional differences are also evident in *tasmin* performance. Most simulations show better agreement with observations over  
398 the MC. In contrast, larger errors over the Mainland suggest greater challenges in representing land-surface processes,  
399 boundary-layer dynamics, and regional circulation influences that strongly affect night time temperature.

400 Since there are large observational uncertainties in temperature variables over Southeast Asia (Fig. S1), the additional results  
401 for multiple reference products are presented in the supplementary material (Fig. S2-S10). It is noted that the temperature from  
402 BEST is higher than any other product. However, the main conclusion remains the same, regardless of the choice of reference.  
403 In summary, cold biases of CMIP6-downscaled RCMs in *tas* primarily originate from deficiencies in simulating *tasmax*, which



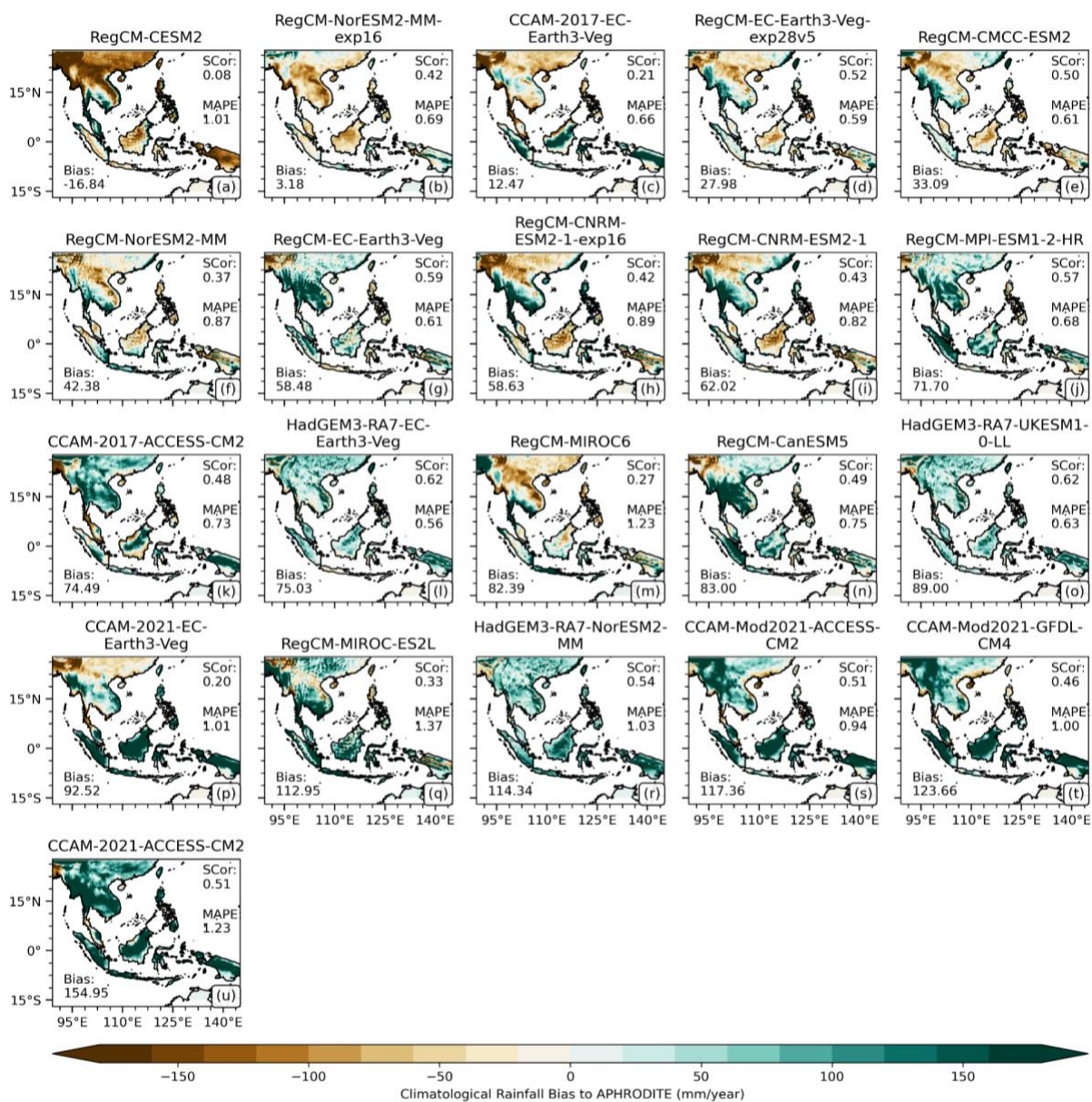
404 exhibits larger magnitude errors and stronger regional and seasonal variability than those in *tas* and *tasmax*. While *tasmin*  
405 biases are generally smaller and more spatially heterogeneous, *tasmax* biases show more systematic and pronounced errors,  
406 particularly over the MC and during JJA. Importantly, across all temperature variables (*tas*, *tasmax*, and *tasmin*), the spatial  
407 structure of biases is strongly determined by the RCM, highlighting the dominant role of regional model physics and  
408 parameterizations in shaping near-surface temperature performance in CORDEX-SEA simulations.

### 409 3.2 Precipitation

410 We then compared the seasonal mean total precipitation on wet days from RCM simulations (1982–2014) against  
411 APHRODITE (Figs. 6-7). Precipitation biases exhibit larger spatial and inter-RCM variability than temperature biases. Most  
412 models capture the spatial distribution of precipitation reasonably well, with 16 out of 21 simulations showing spatial  
413 correlations exceeding 0.4. In terms of regional averages, almost all RCMs exhibit wet biases for MJJASO total precipitation,  
414 ranging from 3.18 mm yr<sup>-1</sup> to 158.95 mm yr<sup>-1</sup>. The only exception is RegCM-CESM2, which shows a dry bias of -16.84 mm  
415 yr<sup>-1</sup> and a low spatial correlation score of 0.08.

416 Despite generally reasonable spatial correlations, precipitation bias patterns are highly spatially heterogeneous, characterized  
417 by a combination of wet and dry regions. Distinct groups of RCM-type-related biases can be identified. For instance, CCAM-  
418 2021 and CCAM-2017 simulations exhibit wet biases over topographically complex regions, particularly the MC, where  
419 numerous islands of varying sizes are present. Similarly, biases in HadGEM3-RA7 and CCAM-Mod2021 simulations remain  
420 consistent regardless of the driving GCM, likely due to the bias- and variance-corrected SST forcing, as previously noted by  
421 Evans et al. (2020). In contrast, RegCM's simulations show pronounced wet biases over high wind-speed regions such as  
422 Thailand, along with dry biases over Borneo. Comparison of RegCM5 and RegCM4 simulations forced by EC-Earth3-Veg  
423 shows an improvement in presentation of precipitation with substantial reductions of wet biases over Thailand. Interestingly,  
424 although RegCM-CanESM5 and RegCM-MIROC6 exhibit similar domain-mean biases (approximately 83 mm yr<sup>-1</sup>, Fig. 6),  
425 their spatial bias structures differ markedly. RegCM-CanESM5 shows a predominantly wet bias across most of the domain,  
426 except over the north-western part of SEA, whereas RegCM-MIROC6 exhibits dry biases over much of the domain, with wet  
427 biases confined primarily to north-western Myanmar and southern Thailand. Using the same GCM nudging technique, CCAM-  
428 2017 simulations show significant improvement compared with CCAM-2021. These findings highlight the critical role of  
429 RCM setup in shaping precipitation biases.

430 The pattern of the NDJFMA reveals some interesting features (Fig. 7). RCMs show better skill in capturing the spatial  
431 distribution of precipitation, with dry biases over the mainland and wet biases over MC. Interestingly, the higher biases are  
432 more prone to MC in all simulations. Specifically, the RegCM simulations cannot capture the spatial distribution of  
433 precipitation well over MC, with all models showing a low correlation coefficient of less than 0.2 (figure not shown).

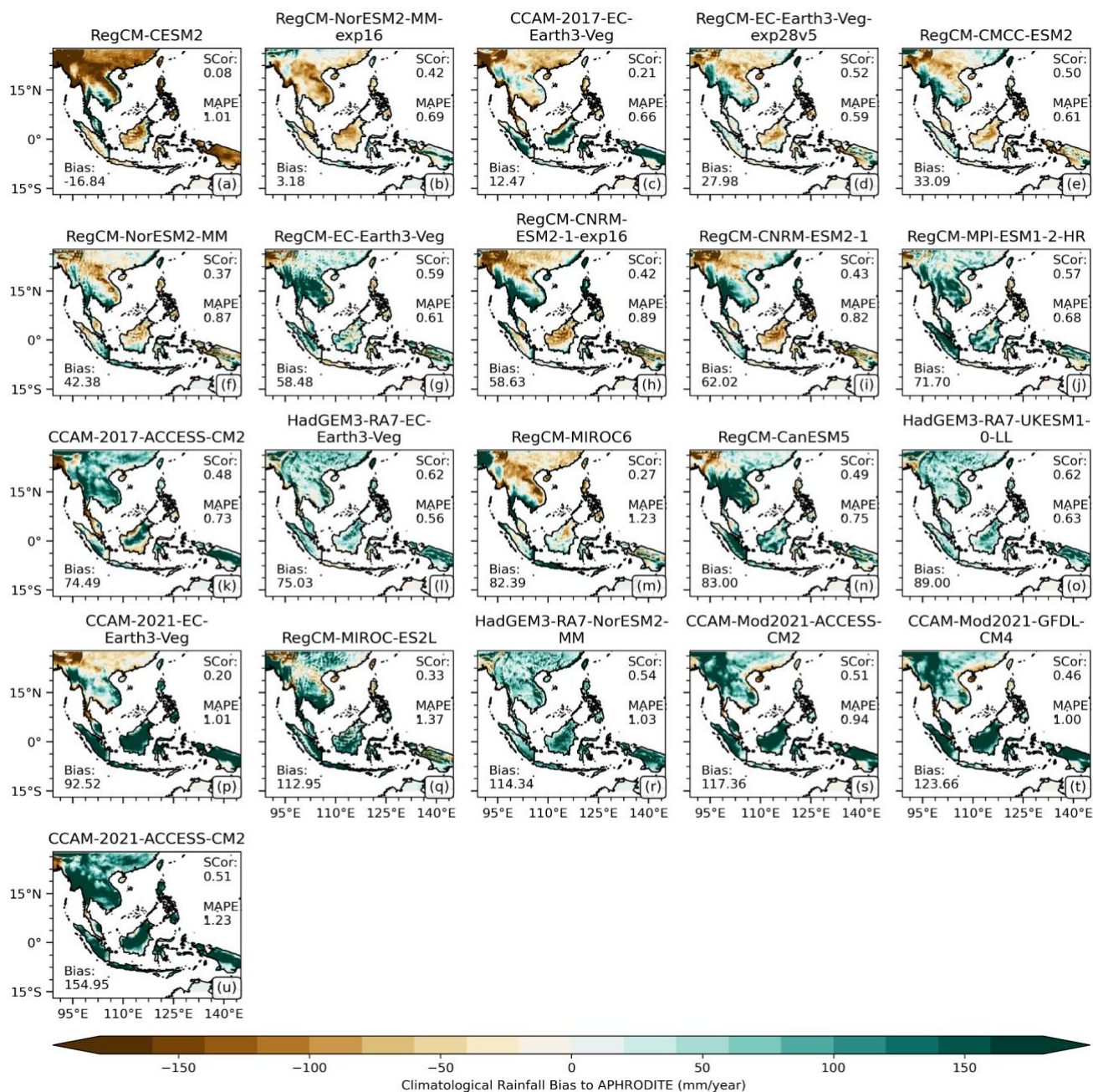


434

435 **Figure 6. Seasonal climatological (1982–2014) biases (in mm yr<sup>-1</sup>) for each model against the APHRODITE observational product**  
 436 **during the May-October (MJJASO) season, ranked from driest to wettest based on regionally averaged bias. The mean absolute**  
 437 **percentage errors (MAPEs) and spatial correlations (Scor) calculated against APHRODITE are shown in the upper-right corner.**  
 438 **All analyses are considered at the resolution of the CORDEX-SEA simulation (i.e., ~ 25 km). The stippled area indicates locations**  
 439 **where RCM shows statistically significant bias (p < 0.05) according to the Mann-Whitney U test.**



NDJFMA Climatological Rainfall Bias (1982-2014) compared to APHRODITE



440

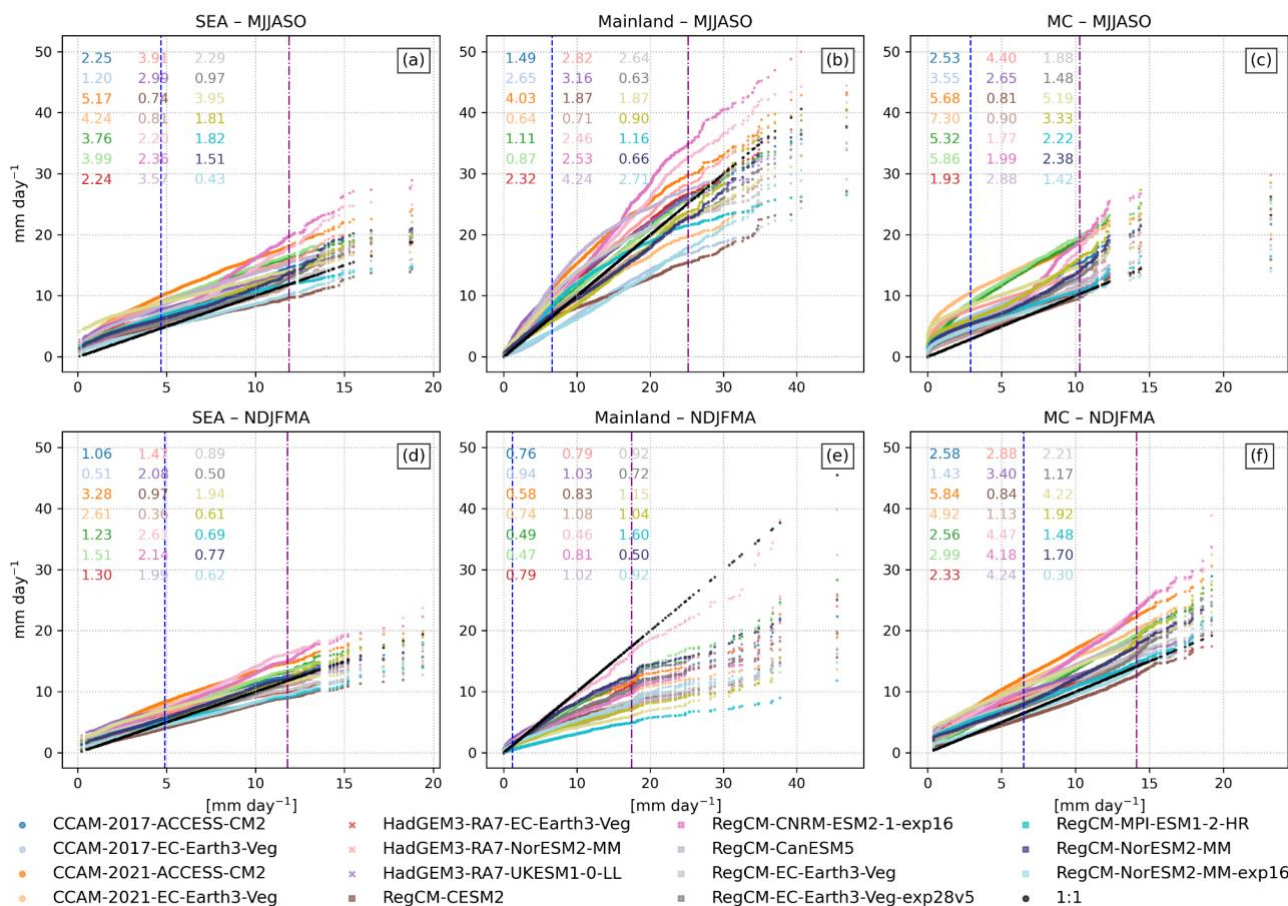
441 **Figure 7. Same as Fig. 6 but for the November–April (NDJFMA) season.**



442 Due to large observational uncertainties in precipitation during both seasons (Fig. S1), the similar analyses of mean bias are  
443 applied for other different observational datasets (Fig. S11). Interestingly, there are at least 14 out of 21 RCM simulations  
444 exhibiting the wet biases in terms of regionally averaged total wet-day precipitation, regardless of the choice of reference data.

445 The seasonal cycle of monthly mean total rainfall over SEA is presented in Fig. S12. Rainfall peaks during May–October over  
446 the Mainland, whereas higher precipitation is observed from November to April across the MC. The RCMs generally reproduce  
447 the peak rainfall over the Mainland; however, most RegCM simulations fail to adequately capture the precipitation peaks over  
448 the MC.

449 Figure 8 compares regionally-averaged daily precipitation quantiles from CORDEX-SEA RCMs with APHRODITE  
450 observations over the whole of SEA, the Mainland, and the MC for the MJJASO and NDJFMA seasons during 1982–2014.  
451 Precipitation is also considered in three percentile ranges: 0–50th percentile (left of the blue dashed line), 50–99th percentile  
452 (between the dashed and dot-dashed lines), and 99th percentile (right of the dot-dashed line), allowing a detailed assessment  
453 of model performance across the distribution.



454

455 **Figure 8. Quantile-quantile plots for regionally averaged daily precipitation (pr, in mm d<sup>-1</sup>) across Southeast Asia for the MJJASO**  
 456 **and NDJFMA seasons during the climatological period of 1982-2014. The inserted number indicated values of the area score metric**  
 457 **(ASM), which measures the proximity between the two distributions: model and observation (APHRODITE). The vertical lines**  
 458 **indicate the 50<sup>th</sup> percentile (blue) and 99<sup>th</sup> percentile (purple), respectively.**

459 Overall, almost all RCM (coloured) lines are above the observational line (black), indicating more intense precipitation in  
 460 simulations except over the Mainland during the NDJFMA season. This systematic shift toward higher precipitation values in  
 461 RCMs compared to APHRODITE is more evident after the 50th percentile. At the highest percentiles, RCMs diverge markedly  
 462 from the reference dataset, highlighting the ongoing challenges for RCMs to capture the intensity of extreme precipitation.  
 463 Note that some RCMs (CCAM-2017-ACCESS-CM2, CCAM-2021-EC-Earth3-Veg) more closely match observed extremes  
 464 during dry seasons, while others remain biased, either overestimating (e.g., RegCM-EC-Earth3-Veg and RegCM-MIROC-  
 465 ES2L) or underestimating (RegCM-CESM2) the heaviest rainfall during the dry seasons. An exception is RegCM-CESM2,  
 466 which has persistent dry biases in the RCM in both seasons. Interestingly, all simulations are below the observational line for



467 the Mainland during DJFMA, indicating the dry biases as mentioned above (Fig. 8e). Quantitative evaluation using the area  
468 score shows that CORDEX-SEA simulation aligns more closely with observations during the dry season compared to the wet  
469 season (17 out of 21 simulations exhibit smaller area scores, regardless of the reference dataset, Fig. S13). Among all  
470 simulations, CCAM-2021-ACCESS-CM2 displays the largest deviations from observations across both seasons, as reflected  
471 in its area scores, which are higher than those of other RCMs.

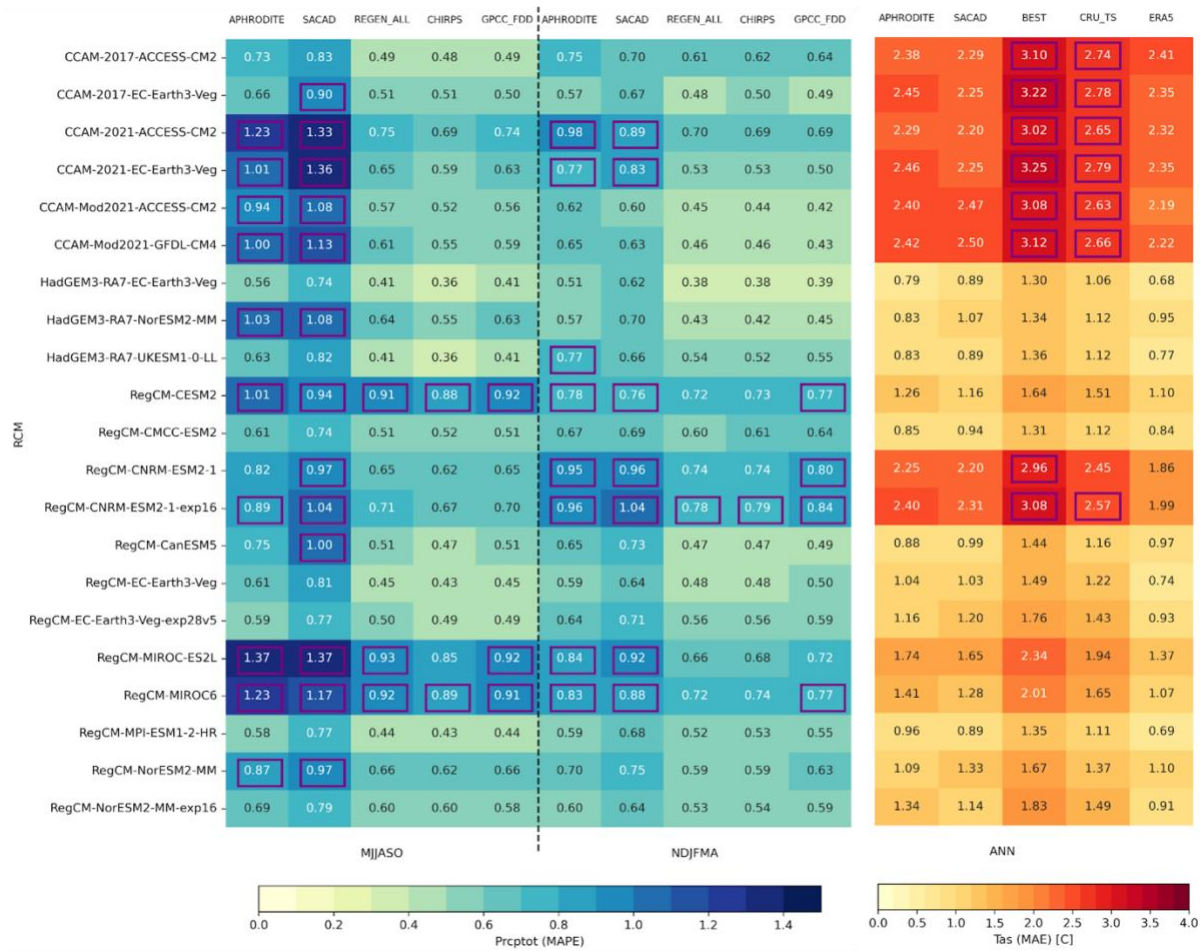
472 There is an interesting difference between the two sub-regions. While the RCMs generally capture precipitation below the 50th  
473 percentile well over the Mainland, the distribution over the MC is more divergent, even at percentiles below the 50th. This  
474 highlights the challenges in simulating precipitation over the MC, which consists of numerous islands of varying sizes and  
475 complex atmospheric-oceanic interactions. Moreover, due to the dominant role of convective rainfall over the MC, this region  
476 is highly sensitive to the cumulus parameterizations schemes used in RCMs (Ngo-Duc et al., 2017)

### 477 **3.3 Benchmarking CMIP6-CORDEX SEA simulations for further downscaling at kilometre-scale**

478 In this section, we move to the next step of subsetting the 21 RCM simulations from the CMIP6 CORDEX-SEA ensemble for  
479 further dynamical downscaling at the kilometre-scale over SEA megacities, under the CARE for SEA megacities project using  
480 the MSMs from the BMF (Isphording et al., 2024).

#### 481 **3.3.1 Spatial benchmark**

482 This benchmarking evaluates the ability of the RCM ensemble to reproduce the magnitude and spatial distribution of observed  
483 precipitation and temperature by comparing model outputs against five reference datasets. The expectation is that models  
484 should not exhibit substantial wet or dry biases in precipitation nor strong cold or warm biases in temperature and should  
485 adequately capture the spatial variability of these core climate variables. Figure 9 presents the mean absolute percentage error  
486 (MAPE) for precipitation during the MJJASO and NDJFMA seasons and the mean absolute error (MAE) for annual  
487 temperature, while Fig. 10 shows the corresponding spatial correlations with multiple reference datasets. Bias metrics are  
488 calculated using absolute percentage errors for precipitation and absolute temperature differences for temperature, ensuring  
489 that positive and negative deviations across grid points do not cancel out. Given the considerable observational uncertainties  
490 in rainfall and temperature (Fig. S1), caution is required when interpreting these bias benchmarks.



491

492

493

494

495

**Figure 9. Score benchmarks for biases in seasonal total precipitation (MAPE: Mean Absolute Percentage Errors) and annual daily mean near-surface temperature (MAE: Mean Absolute Errors) referenced to multiple observational datasets. Biases larger than the benchmark are marked by purple squares. Lighter colours typically indicate better performance, whereas darker colours often indicate worse performance.**

496

497

498

499

500

501

502

At this MSMs stage, we would like to retain as many models as possible to maintain a sufficiently large ensemble for further testing. To account for seasonal variations in model performance, different fixed thresholds were prescribed for wet and dry seasons. In particular, thresholds of 0.85 ( $MAPE \leq 0.85$ ) and 0.75 ( $MAPE \leq 0.75$ ) were applied to the precipitation benchmark for the MJJASO and NDJFMA seasons, respectively while a threshold of 2.5 ( $MAE \leq 2.5$ ) was used for the temperature benchmark. Note that similar strategies to identify these thresholds were adopted from Nguyen et al. (2024), who benchmarked CMIP6 model performance to select a subset of GCMs for dynamical downscaling purposes over SEA. More relaxed thresholds were applied here due to the smaller number of RCMs considered compared with the number of GCMs. Similarly,



503 for spatial correlation metric (Scor), thresholds of 0.3 and 0.5 were applied for precipitation during the MJJASO and NDJFMA  
504 seasons, respectively, while 0.8 is applied for annual mean temperature.

505 Figure 9a illustrates the sensitivity of the intensity benchmark (MAPE) to different precipitation reference datasets. For  
506 instance, when regional datasets such as APHRODITE and SACA&D are used as references, at least ten models exceed the  
507 benchmark thresholds. These include the CCAM-2021 and CCAM-Mod2021 simulations, HadGEM3-RA7-NorESM2-MM,  
508 RegCM-CESM2, RegCM-CNRM-ESM2-1-exp16, RegCM-MIROC-ES2L, RegCM-MIROC6, and RegCM-NorESM2-MM.  
509 It is worth noting that although regional datasets incorporate a greater number of gauge stations than global products, they tend  
510 to be drier in both mean and extreme precipitation (Alexander et al., 2025; Nguyen et al., 2020; Yatagai et al., 2012). A subset  
511 of models consistently fails the intensity benchmark—exceeding thresholds for at least three references. datasets—regardless  
512 of the reference used. These include RegCM-CESM2, RegCM-MIROC-ES2L, and RegCM-MIROC6 in both seasons, as well  
513 as RegCM-CNRM-ESM2-1-exp16 and RegCM-CNRM-ESM2-1 during the dry season. In contrast, temperature exhibits less  
514 sensitivity across reference datasets. Several models, including the six CCAM simulations, RegCM-CNRM-ESM2-1, and  
515 RegCM-CNRM-ESM2-1-exp16, still show MAE exceeding 2°C irrespective of the reference dataset. This might result from  
516 the consistent cold biases across all grids in these models.

517 Figure 10 shows that nearly all models pass the spatial variability benchmark for temperature, with spatial correlations  
518 exceeding 0.8. Note that CCAM's simulations have a lower spatial correlation with SACAD (e.g., less than 0.8) than other  
519 references. Only two models, RegCM-CESM2 and RegCM-MIROC6, fail to capture the spatial contrast of precipitation in  
520 either or both seasons, regardless of the reference dataset used.

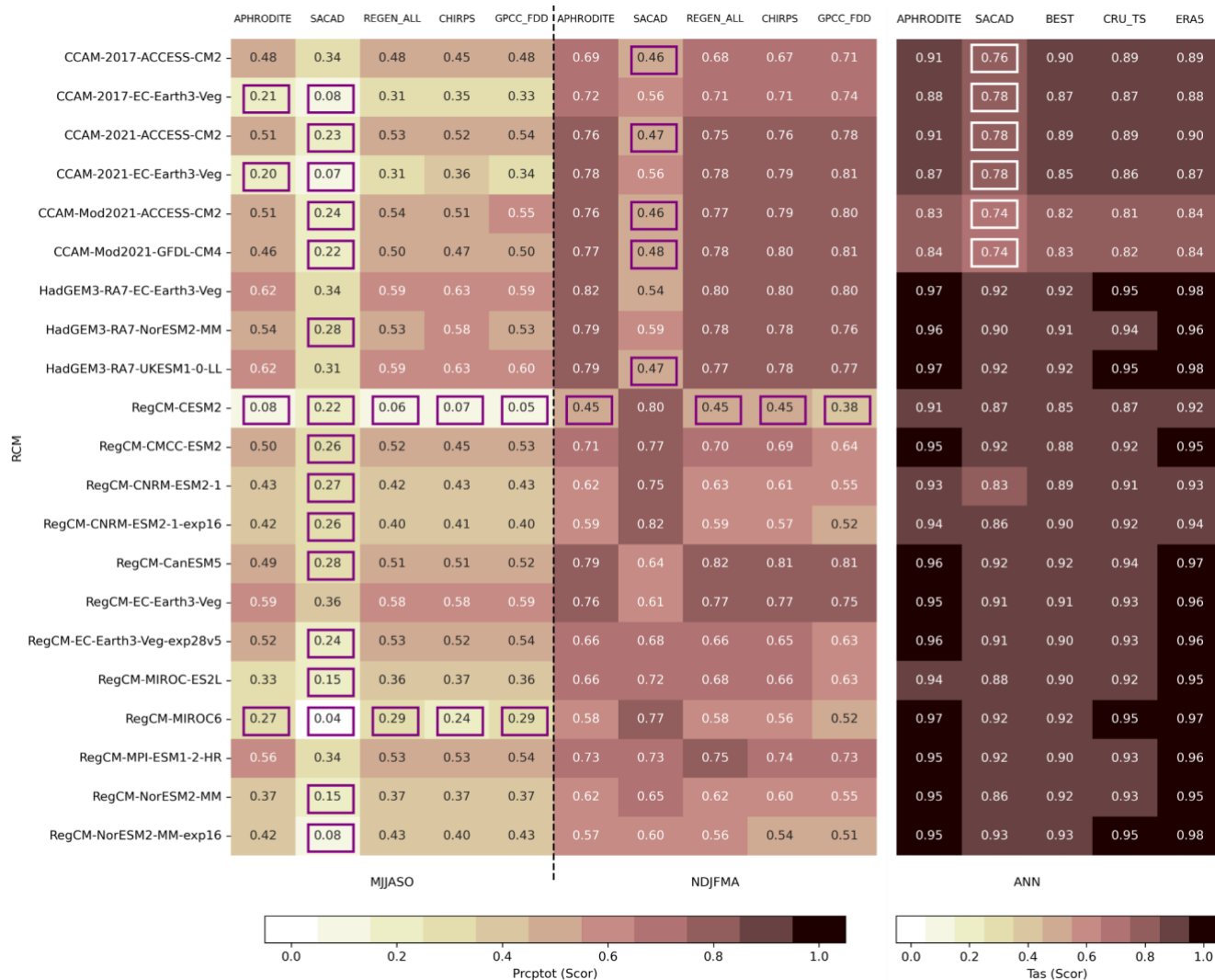


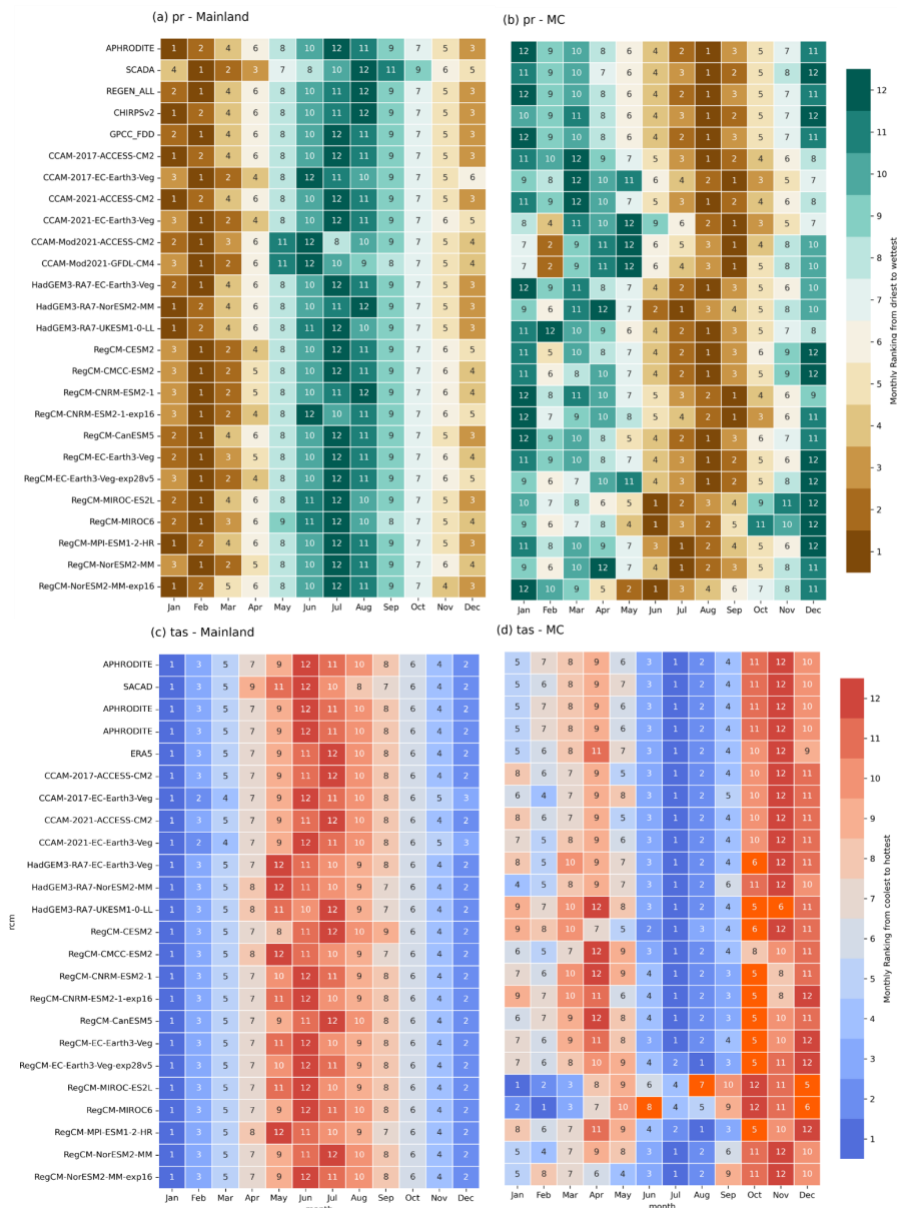
Figure 10. Score benchmarks for spatial correlation of seasonal total precipitation (preptot) and annual daily mean near-surface temperature (tas) with multiple observational datasets. Scores less than the benchmark are marked by squares. Darker colors typically indicate better performance, whereas lighter colors typically indicate worse performance.

### 3.3.2 Seasonal cycle benchmark

The seasonal cycle benchmark follows the recommendation of Ispording et al. (2024) for unimodal seasonal patterns. This criterion requires that the three-month observed low and high peaks occur within the modeled lowest and highest six months of the year, respectively. The benchmark was applied to both precipitation and temperature and evaluated separately for two sub-regions to reflect differences in the timing of seasonal peaks. Figure 11 presents the months satisfying this benchmark for



530 each variable. Colors and numbers denote the ranking of months from driest/coldest (1) to wettest/hottest (12), based on  
 531 observed seasonal cycles derived from all reference datasets.



532  
 533 **Figure 11. Seasonal cycle benchmark following Ishphoring et al. (2024) for unimodal seasonal cycle of (a-b) precipitation (pr) and**  
 534 **(c-d) near-surface mean temperature (tas) in the Mainland and MC. Colors and numbers indicate the ranking for latitude-weighted**  
 535 **monthly total precipitation/daily temperature, with 1 being the driest/coldest and 12 being the wettest/hottest. The values highlighted**  
 536 **in orange indicate that the simulation does not meet our benchmarking expectations.**



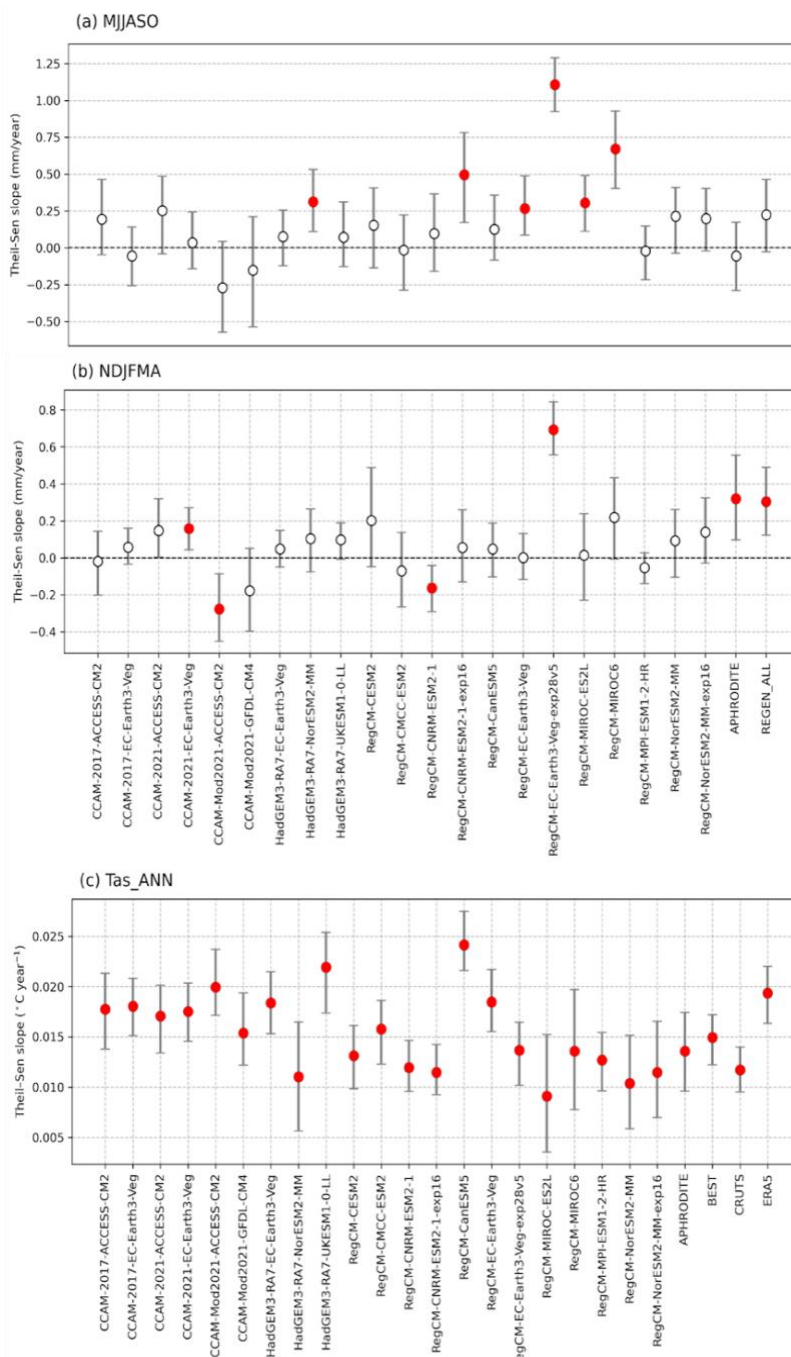
537 Observations reveal consistent timing of seasonal peaks: the wettest period occurs from June to August over the Mainland and  
538 from December to April over the MC, corresponding to the prevailing monsoon regimes. For temperature, the hottest months  
539 occur in June–August over the mainland and in October–December over the MC.

540 Overall, all models meet the precipitation benchmark across both sub-regions. However, some RegCM simulations display a  
541 weaker representation over the MC, with anomalously dry months during the observed wet season. As shown in Fig. S12, this  
542 discrepancy arises from shifts in the simulated low and high rainfall peaks. For temperature, all models satisfy the benchmark  
543 over the Mainland, which exhibits a clear unimodal cycle. In contrast, 11 of 21 simulations fail to capture the observed solar-  
544 irradiance peak in November–December (ranks 11–12) over the MC, instead simulating cooler conditions around ranks 5–6.  
545 Given the bimodal temperature cycle over the MC (Section 3.1), this benchmark is not strictly applicable there; thus, all models  
546 are considered to pass for temperature over the MC.

### 547 **3.3.3 Long-term trend benchmark**

548 This benchmark is based on the expectation that simulating observed large-scale climate variability and change is crucial for  
549 climate change adaptation. Trends were considered in terms of time series of regional-averaged total precipitation and  
550 temperature, rather than at a single grid, given the substantial variability arising from small-scale processes or model  
551 parameterizations, which may not be robust across models or observational datasets.

552 To reduce the impact of decadal variability, we have extended the full historical period, from 1960 to 2014. The trend is  
553 estimated using a Theil-Sen slope estimator (Theil, 1950; Sen, 1968). Confidence intervals are computed with a significant  
554 value of  $p < 0.05$ . Confidence intervals are marked as error bars on Fig. 12 for reference-based values and for all simulations.  
555 We test the significance of the trend using the Mann-Kendall significance test at the 5% level (Hussain and Mahmud, 2019).



556  
 557 **Figure 12. Trend estimated based on the Theil-Sen slope estimator of the time series of seasonal total wet-day precipitation (a–b)**  
 558 **and annual near-surface mean temperature (c) among models and observations. The red dot indicates a significant trend, as**  
 559 **determined by the Mann-Kendall test at a 5% level of confidence. The bar indicates 90% confidence intervals.**



560 Figures 12a–b show the long-term trend for the annual time series of seasonal average total precipitation, while Fig. 12c shows  
561 the trend for the annual time series of annual average daily mean near-surface temperature. In terms of total wet-day  
562 precipitation, APHRODITE and REGEN\_ALL show different directions in the long-term MJJASO trend, although neither  
563 trend is significant (Fig. 12a). It is acknowledged that APHRODITE was merged from two versions (see Sect. 2.2), which  
564 have slight differences in data sources and algorithms for periods before and after 2007; thus, trends in APHRODITE should  
565 be considered with care. Our benchmarking threshold is therefore “no trend” (since neither one of the observed datasets has a  
566 significant trend), and all RCM simulations pass this benchmark during the MJJASO season. Meanwhile, during the NDJFMA  
567 season, most RCM simulations underestimate the magnitude of the observed positive trends found in APHRODITE and  
568 REGEN\_ALL (e.g., 0.36 and 0.32 mm/year, respectively, Fig. 12b). All RCMs pass the trend benchmark for the dry season  
569 except RegCM-CNRM-ESM-1-2 and CCAM-Mod2021-ACCESS-CM2, which have significant negative trends. Note that in  
570 both seasons, the confidence interval in observations and models is quite wide, reflecting an uncertain change signal. For  
571 temperature, all models and references show a significant increasing trend, coincident with global warming. Therefore, only  
572 two models: RegCM-CNRM-ESM2-1 and CCAM-Mod2021-ACCESS-CM2, fail this benchmark.

573 Note that IPCC AR6 [Chapter 11, Seneviratne et al. (2021)] documented a positive precipitation trend over the MC after 1980  
574 with high confidence. Therefore, we also conducted additional trend tests over a shorter 33-year time period (1982 to 2014),  
575 coinciding with the availability of all reference products (Figs. S14–S15). Although the trends in observations vary from non-  
576 significant to significant positive for precipitation, no model fails this benchmark. Although these results somehow contrast  
577 the trend analysis over a longer period, RegCM-CNRM-ESM2-1 and CCAM-Mod2021-ACCESS-CM2 fail another  
578 benchmark, so they are still removed from further analysis.

579 Table 4 summarises the results of 21 CMIP6 CORDEX-SEA simulations using the MSM from BMF. At the point of applying  
580 BMF, we find 15 simulations (highlighted by blue in Table 4) that meet our expectations in simulating the fundamental  
581 characteristics of precipitation and temperature over Southeast Asia.

582

583

584

585

586



587  
588

**Table 4. Summary of the BMF results. An “x” denotes models that pass the benchmark, while “-” indicates models that do not pass the benchmark.**

Model	precipitation							temperature				Total
	MJJASO			NDJFMA			Scyl	ANN				
	MAPE	Scor	Trend	MAPE	Scor	Trend		MAE	Scor	Scyl	Trend	
CCAM-2017-ACCESS-CM2	x	x	x	x	x	x	x	x	x	x	x	11
CCAM-2017-EC-Earth3-Veg	x	x	x	x	x	x	x	x	x	x	x	11
CCAM-2021-ACCESS-CM2	x	x	x	x	x	-	x	x	x	x	x	10
CCAM-2021-EC-Earth3-Veg	x	x	x	x	x	x	x	x	x	x	x	11
CCAM-Mod2021-ACCESS-CM2	x	x	x	x	x	x	x	x	x	x	x	11
CCAM-Mod2021-GFDL-CM4	x	x	x	x	x	x	x	x	x	x	x	11
HadGEM3-RA7-EC-Earth3-Veg	x	x	x	x	x	x	x	x	x	x	x	11
HadGEM3-RA7-NorESM2-MM	x	x	x	x	x	x	x	x	x	x	x	11
HadGEM3-RA7-UKESM1-0-LL	x	x	x	x	x	x	x	x	x	x	x	11
RegCM-CESM2	-	-	x	-	-	x	x	x	x	x	x	7
RegCM-CMCC-ESM2	x	x	x	x	x	x	x	x	x	x	x	11
RegCM-CNRM-ESM2-1	x	x	x	-	x	-	x	x	x	x	x	9
RegCM-CNRM-ESM2-1-exp16	x	x	x	-	x	x	x	x	x	x	x	10
RegCM-CanESM5	x	x	x	x	x	x	x	x	x	x	x	11
RegCM-EC-Earth3-Veg	x	x	x	x	x	x	x	x	x	x	x	11
RegCM-EC-Earth3-Veg-exp28v5	x	x	x	x	x	x	x	x	x	x	x	11
RegCM-MIROC-ES2L	-	x	x	x	x	x	x	x	x	-	x	9
RegCM-MIROC6	-	x	x	-	x	x	x	x	x	-	x	8
RegCM-MPI-ESM1-2-HR	x	x	x	x	x	x	x	x	x	x	x	11
RegCM-NorESM2-MM	x	x	x	x	x	x	x	x	x	x	x	11
RegCM-NorESM2-MM-exp16	x	x	x	x	x	x	x	x	x	x	x	11

589

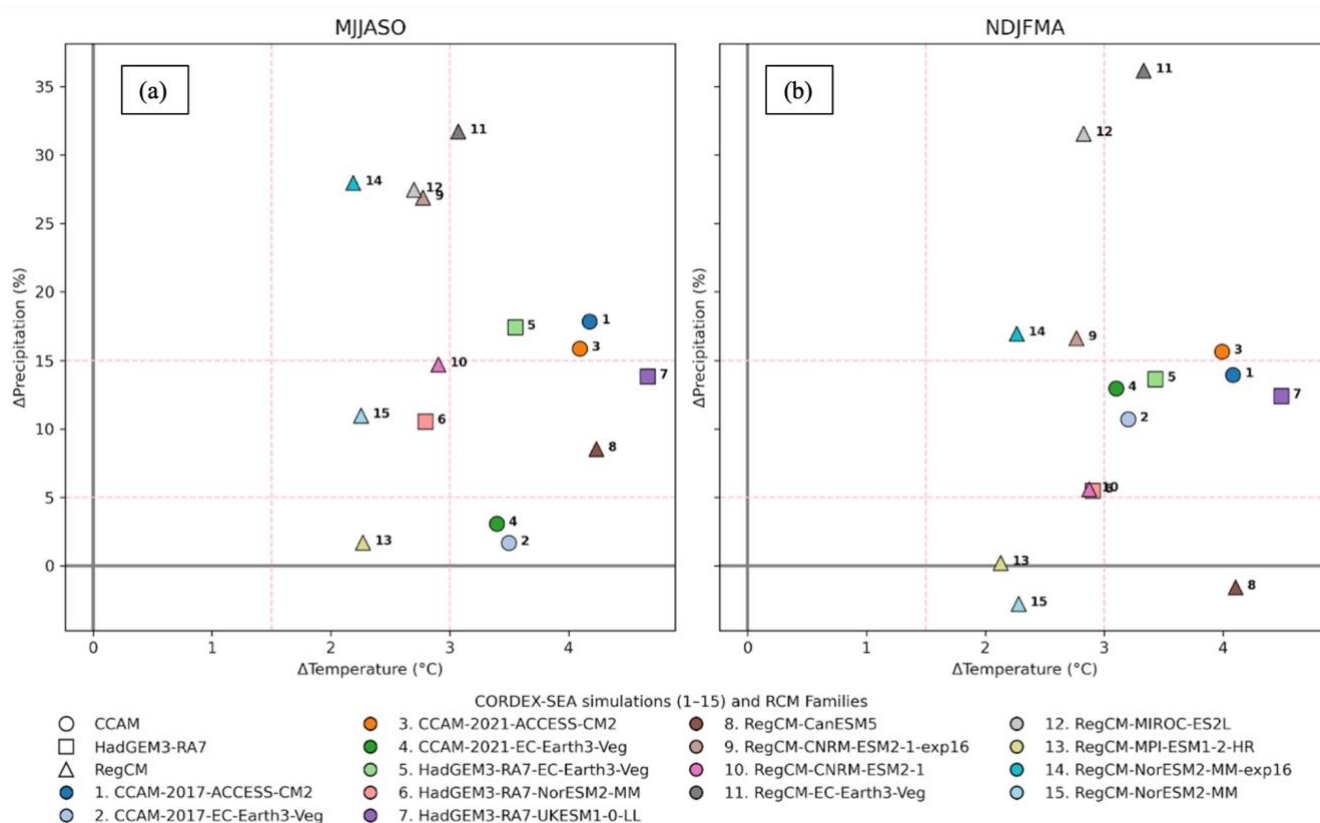
590 **3.4 Future climate change signal and model dependence.**

591 In this section, we examine the projected future climate change spread from the CMIP6 CORDEX-SEA ensemble, which  
 592 provides simulations under the SSP3-7.0 scenario (Table 1). Fig. 13 shows the distribution of projected changes in mean  
 593 precipitation (y-axis) versus mean temperature (x-axis) during the wet and dry seasons. In this study, we classify regional  
 594 temperature change into low, medium, and high warming categories. Specifically, low, medium, and high regional warming  
 595 are defined as regional mean temperature increases of approximately +1.5°C, +2°C, and > +3°C relative to the baseline period



596 (1981–2010), respectively. Meanwhile, precipitation thresholds are set at dry (below 5%), neutral (5–15%), and wet (above  
597 15%), respectively.

598 In general, both variables exhibit an increasing tendency, with temperature changes sitting in the mid to high ranges (e.g.,  
599 changes from 2 to 5°C) and precipitation changes from 1.5 to 35%. However, several RegCM experiments (RegCM-MPI-  
600 ESM1-2-HR, RegCM-NorESM2-MM, and RegCM-CanESM5) indicate decreasing trends in daily precipitation during  
601 NDJFMA, despite lying within the mid- to low-range precipitation projections during MJJASO.



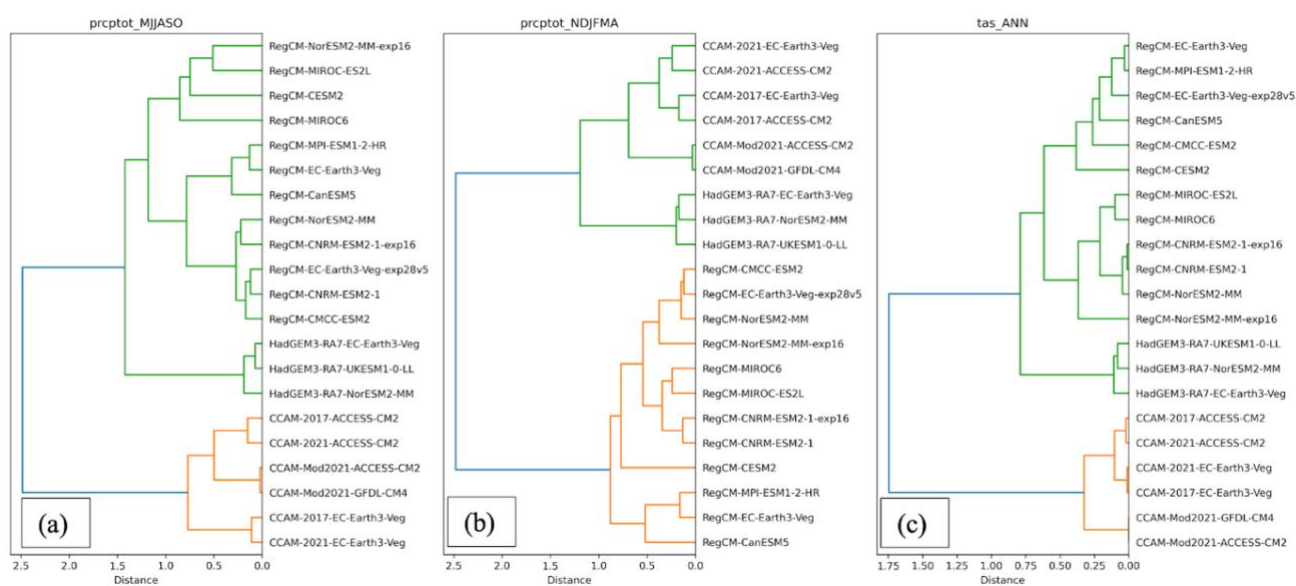
602  
603 **Figure 13. CMIP6 CORDEX-SEA ensemble future spread (2070–2099 relative to 1981–2010) over the land of Southeast Asia during**  
604 **(a) the MJJASO and (b) the NDJFMA seasons. The analysis is conducted for simulations that are available for SSP3-7.0 scenarios**  
605 **(Table 1). Vertical and horizontal dashed red lines indicate threshold values used to separate low, medium, and high ranges of**  
606 **projected temperature and precipitation changes. Temperature thresholds are set at +1.5°C, +2°C, and >+3°C, and precipitation**  
607 **thresholds are set at dry: <5%, neutral: 5–15%, and wet: >15%, respectively.**

608 Among the 15 models passing the BMF criteria, 11 experiments provide SSP3-7.0 simulations. These experiments cluster  
609 around the mid-range of temperature projections but span a wide range of precipitation responses. Wet models projecting  
610 precipitation increases include RegCM-EC-Earth3-Veg, RegCM-NorESM2-MM-exp16 (e.g. above 15%), CCAM-2017-



611 ACCESS-CM2, CCAM-2021-ACCESS-CM2, HadGEM3-RA7-EC-Earth3-Veg, HadGEM3-RA7-NorESM2-MM,  
 612 HadGEM3-RA7-UKESM1-0-LL, and RegCM-NorESM2-MM (e.g., 5–15%); while no or dry changes (< 5%) are represented  
 613 by CCAM-2017-EC-Earth3-Veg, RegCM-MPI-ESM1-2-HR, and RegCM-CanESM5.

614 The dendrograms from hierarchical clustering of historical precipitation and mean temperature (Fig. 14) reveal three dominant  
 615 spatial clusters, broadly corresponding to the RCM families, including CCAM, HadGEM3-RA7, and RegCM for MJJASO  
 616 precipitation and annual mean temperature patterns (Figs. 14a, c). In contrast, the NDJFMA precipitation pattern (Fig. 14b)  
 617 forms two primary branches separating CCAM/HadGEM3-RA7 and RegCM simulations, highlighting the seasonal  
 618 dependence of clustering results, consistent with Nguyen et al. (2024) and Gibson et al. (2023).



619  
 620 **Figure 14. Dendrogram with hierarchical clustering of spatial patterns of historical seasonal total wet-day precipitation (a-b) and**  
 621 **annual daily mean temperature (c). Colours indicate the different cluster assignments. The horizontal axis on the dendrogram is a**  
 622 **measure of similarity between individual models and clusters, where models aligned on the same branches have similar spatial**  
 623 **patterns.**

624 Overall, based on model performance, future spread, model dependency, and data availability, we select at least two  
 625 experiments from three independent model groups to be considered for further km-scale dynamical downscaling over SEA  
 626 megacities. These include:

- 627 ▪ RegCM: EC-Earth3-Veg – high range; NorESM2-MM – mid range; MPI-ESM1-2-HR and CanESM5 – low range
- 628 ▪ HadGEM3-GA7: EC-Earth3-Veg and UKESM1-0-LL—mid-range; and
- 629 ▪ CCAM-2017: ACCESS-CM2 – mid-range; EC-Earth 3-Veg – low range



#### 630 4. Discussion and Conclusions

631 The overall aims of this study were to (1) document the experimental design for producing the updated CMIP6 dynamical  
632 downscaled climate simulations for Southeast Asia (SEA); (2) comprehensively assess model performance over the historical  
633 period across climatological fields of model core variables: daily precipitation, near-surface temperature (*tas*), daily maximum  
634 temperature (*tasmax*), and daily minimum temperature (*tasmin*); and (3) select a subset of RCMs for further dynamical  
635 downscaling at km-scale over five megacities in SEA based on benchmarking model performance, model independence, and  
636 a range of future model responses.

637 Observational uncertainties are an important aspect in the context of model evaluation and benchmarking. Over SEA,  
638 observations are sparse and have large uncertainties (Nguyen et al., 2020; Alexander et al., 2020), complicating model  
639 assessment and benchmarking (Nguyen et al., 2024). Note that the observational uncertainties are quite large compared with  
640 benchmarks, reaching greater than 50% of benchmarking errors (MAPE and MAE) in the wet season for total precipitation  
641 and for temperature at annual scales, particularly over the MC (Table S1). Therefore, benchmarking based on MJJASO  
642 seasonal rainfall and annual mean temperature should be interpreted with caution. Uncertainty in spatial correlation is low for  
643 both temperature and rainfall, ranging from 2% to 10% of the benchmarking values. On the other hand, all observational  
644 products show a similar trend (Fig. 12 and Figs. S14-S15) and seasonal cycle (Figs. S4 and S12 for temperature and  
645 precipitation, respectively). To deal with observational uncertainty, model biases are reassessed with multiple observations  
646 from different sources (e.g., in situ, blended satellite, and reanalysis datasets; global and high-resolution regional gridded  
647 datasets). The following are key findings of this evaluation:

648 (1) Despite the large observational uncertainties in precipitation intensity, the CMIP6-downscaled CORDEX-SEA ensemble  
649 captures the spatial contrast and temporal mean precipitation distribution over SEA reasonably well but tends to substantially  
650 overestimate observed precipitation (e.g., at least 14 out of 21 models regardless of the choice of observed reference). The  
651 magnitude of biases is both regionally and seasonally heterogeneous, with larger wet biases over regions and seasons  
652 dominated by the prevailing monsoon (e.g., over the MC during NDJFMA and over the Mainland during MJJASO). These  
653 wet biases are particularly pronounced in the CCAM and HadGEM3-RA7 simulations. This requires further investigation into  
654 process-based metrics for precipitation drivers (e.g., monsoon) in the RCM ensemble.

655 (2) The CMIP6 CORDEX-SEA ensemble reproduces the observed spatial distribution of temperature reasonably well but  
656 generally exhibits cold biases, particularly over the Mainland and during the boreal winter (DJF) season, as well as in  
657 simulations that overestimate precipitation (e.g., CCAM and HadGEM3-RA7 simulations). Comparisons with the BEST,  
658 SACAD and CRU TS datasets indicate that these cold biases are primarily linked to an underestimation of *tasmax* rather than  
659 *tasmin*. This finding is consistent with previous studies (Schroeter et al., 2024; Chapman et al., 2023), which reported persistent



660 cold biases in CCAM simulations of *tasmax*—most notably over northern Australia during the wet season—potentially  
661 associated with an overestimation of high-level cloud cover. In contrast, ERA5 displays an opposite pattern, with biases mainly  
662 arising from the underestimation of *tasmin* (Figs. S2 and S7). Further investigation is therefore warranted. Overall, the regional  
663 models demonstrate higher skill in simulating temperature characteristics than precipitation over SEA. This is consistent with  
664 findings from CMIP6 performance assessments over SEA (Nguyen et al., 2024) and from studies in other regions, such as  
665 over Australia (Evans et al., 2021) and Africa (Dosio et al., 2015), where the climate models generally reproduce temperature  
666 more reliably than precipitation, which remains more challenging due to its strong dependency on convection, local processes,  
667 and topography.

668 (3) Comparisons among simulations driven by the same GCM or originating from the same RCM family reveal that runs from  
669 a given RCM family often exhibit similar spatial patterns and bias characteristics. This indicates that RCM configuration exerts  
670 a stronger influence on model biases than the choice of driving GCM. This is inline with previous studies on CMIP5-  
671 downscaled simulations over SEA (Nguyen et al., 2022) or over other CORDEX domains, e.g., Australia (Di Virgilio et al.,  
672 2025), Europe (Kotlarski et al., 2014; Vautard et al., 2021). Within the CMIP6 CORDEX-SEA ensemble, the CCAM-2017  
673 simulations outperform the CCAM-2021 versions. Meanwhile, the RegCM5 simulation forced by EC-Earth3-Veg shows  
674 notable improvements in reducing wet biases compared with RegCM4. These results are based on analyses of a 33-year  
675 climatological period (1982–2014), which differs from Ngo-Duc et al. (2024), who reported no clear improvement in RegCM5  
676 relative to RegCM4-NH based on 5-year ERA5-forced simulations. The discrepancies likely arise from the length of the  
677 evaluation period. As only one EC-Earth3-Veg–forced RegCM5 simulation is currently available, additional RegCM5  
678 simulations with the same forcing GCMs could be further conducted to confirm these improvements compared to RegCM4  
679 and enable more robust intercomparison.

680 (4) The MC remains a particularly challenging region due to its complex geography, consisting of numerous small islands and  
681 steep topography. Consequently, models struggle to accurately capture the spatial variability of rainfall and the internal  
682 variability of key climate variables (e.g., the seasonal cycle of near-surface temperature).

683 Given the goal of selecting RCM simulations to be considered for km-scale dynamical downscaling over SEA megacities, we  
684 applied a novel benchmarking framework (BMF)—a systematic approach designed to identify a subset of fit-for-purpose  
685 models that meet predefined performance expectations. We acknowledge that whether a model passes the BMF depends on  
686 how these performance expectations and reference datasets are defined. Therefore, the benchmarking thresholds were  
687 developed in consultation with model developers and regional stakeholders within CORDEX-SEA, using multiple  
688 observational references. Importantly, assessment against a single reference dataset was not considered sufficient for model  
689 inclusion or exclusion. Instead, a model was excluded only if its skill scores exceeded predefined thresholds for at least half  
690 of the reference datasets (i.e., three out of five in this study).



691 It is worth noting that Nguyen et al. (2024) also established performance thresholds for CMIP6 GCMs to identify models that  
692 meet regional performance expectations over SEA, particularly in simulating precipitation, its key drivers, and associated  
693 teleconnections. However, since the number of RCM simulations in this study is smaller than the GCM ensemble used by  
694 Nguyen et al. (2024) (e.g., 32 CMIP6 GCMs), slightly more relaxed performance thresholds were adopted. In addition, the  
695 objective here is to select suitable RCMs for km-scale downscaling rather than to assess whether RCMs outperform their  
696 driving GCMs.

697 All RCMs were evaluated using Minimum Standard Metrics (MSMs) for *tas* and precipitation, resulting in 15 of 21 simulations  
698 meeting the BMF. Subsequent assessments of model independence revealed strong similarities among simulations from the  
699 same RCM family. Analysis of the projected future response spread led to the identification of three independent model groups  
700 suitable for further downscaling: RegCM (EC-Earth3-Veg, MPI-ESM1-2-HR, CanESM5, and NorESM2-MM); HadREM3-  
701 GA7 (EC-Earth3-Veg and UKESM1-0-LL); and CCAM-2017 (EC-Earth3-Veg and ACCESS-CM2). These selected models  
702 best align with our performance-based expectations and provide a balanced representation of regional processes for future  
703 high-resolution downscaling across the five megacities of Southeast Asia. We do note that benchmarking was done at a regional  
704 scale (e.g., over the Mainland, MC, and SEA) rather than at a city scale, considering the limited availability of reliable  
705 observational datasets in the SEA megacities. Recognizing the high climate variability in SEA, supplementary analysis can  
706 also be done for subdomains or specific areas of interest in SEA.

707 This study presents the first assessment of the CMIP6 CORDEX-SEA ensemble, with a focus on individual ensemble member  
708 performance rather than ensemble mean skill in simulating a range of climate variables. This will improve the utility of CMIP6  
709 CORDEX-SEA projections for climate services by clarifying the reliability and robustness of different RCM families. By  
710 identifying the strengths and weaknesses of each model, we contribute to the ongoing efforts of regional climate modelling,  
711 highlighting the key processes, variables, and sub-regions that require improvement. These insights inform the future model  
712 development while supporting more informed decision-making at the regional scale. We also introduce a case study in which  
713 we utilize the assessment results to select models for further downscaling over SEA megacities, supporting climate risk  
714 assessment for climate adaptation and mitigation over these urban areas. Notably, Singapore's Third National Climate Change  
715 Study [V3; CCRS (2024)] has recently provided high-resolution climate change projections for Singapore and the broader  
716 SEA region through dynamic downscaling of coarse-resolution CMIP6 simulations. The framework developed in this study  
717 can be readily applied as additional ensemble members become available, particularly considering the recent inclusion of V3  
718 data in CORDEX-SEA.



719 **Code and data availability**

720 Code for benchmarking the CMIP6-downscaled CORDEX-SEA performance (Isphording, 2024) is available  
721 from <https://doi.org/10.5281/zenodo.8365065> (Isphording, 2023). CMIP6-downscaled CORDEX-SEA simulation data used  
722 in this study is planned to be published in 2026 through ESGF/NCI.

723 APHRODITE version V1101R1 and V1101 XR (Yatagai et al., 2012) are available  
724 at <https://www.chikyu.ac.jp/precip/english/index.html>.

725 SCA&DA is available at <https://sacad.bmkg.go.id/> (Van Den Besselaar et al. (2017)

726 CRU TS4.08 is available at <https://crudata.uea.ac.uk/cru/data/hrg/> (Harris et al. 2020)

727 ERA5 (Hersbach et al., 2020) is available at <https://doi.org/10.24381/cds.bd0915c6> (Hersbach et al., 2023)

728 BEST data is available at <https://berkeleyearth.org/data/> (Rohde and Hausfather et al., 2020)

729 CHIRPs-v2, REGEN\_ALL, and GPCC\_FDD\_2022 are extracted from the FROGs database (Roca et al., 2019) and available  
730 at <https://frogs.ipsl.fr/>.

731 **Author contributions**

732 PLN and LVA designed the study, carried out the analysis, and wrote the initial manuscript draft. Other co-authors provided  
733 supervision and contributed to manuscript review and revisions.

734 **Competing interests**

735 The contact author has declared that none of the authors has any competing interests.

736

737 **Acknowledgment**

738 UNSW-CCRC CCAM experiments were performed on the computational facility of the National Computational Infrastructure  
739 (NCI) through the UNSW HPC Scheme (DOI: 10.26190/PMN5-7J50). We would also like to thank the NCI HPC (Gadi) for  
740 the computational resources.

741 **Financial support**

742 PLN and LVA are supported by Australian Research Council (ARC) grant FT210100459. LVA is also supported by ARC  
743 grant CE230100012. TND is supported by the Vietnam National Foundation for Science and Technology Development  
744 (NAFOSTED) under Grant 105.06-2021.14. FC, JMD and JT are supported by the “High-Definition Clean Energy, Climate,



745 and Weather Forecasts for the Philippines” project of the Manila Observatory. The downscaled CMIP6 data were obtained  
746 from the SEACLID/CORDEX-SEA project funded by the Asia Pacific Network for Global Change Research (CRRP2023-  
747 08MY-Cruz).

## 748 **References**

749 Alexander, L. V., Bador, M., Roca, R., Contractor, S., Donat, M. G., and Nguyen, P. L.: Intercomparison of annual precipitation  
750 indices and extremes over global land areas from in situ, space-based and reanalysis products, *Environmental Research Letters*,  
751 15, 055002, 10.1088/1748-9326/ab79e2, 2020.

752 Alexander, L. V., Nguyen, P. L., Donat, M. G., Dunn, R. J. H., Tett, S., Zhang, X., Alves, L. M., Bador, M., Deng, X., Gibson,  
753 P. B., King, A., Lennard, C., Min, S.-K., Roca, R., and Trewin, B.: Less Intense Daily Precipitation Maxima in Regional  
754 Compared to Global Gridded Products, *Journal of Climate*, 38, 7669-7693, <https://doi.org/10.1175/JCLI-D-25-0222.1>, 2025.

755 APN: Climatic hazard assessment to enhance resilience against climate extremes for Southeast Asian megacities (CARE for  
756 SEA megacities), <https://doi.org/10.30852/p.26687>, 2023.

757 Best, M. J., Pryor, M., Clark, D., Rooney, G. G., Essery, R. L., Ménard, C., Edwards, J., Hendry, M., Porson, A., and Gedney,  
758 N.: The Joint UK Land Environment Simulator (JULES), model description–Part 1: energy and water fluxes, *Geoscientific*  
759 *Model Development*, 4, 677-699, 2011.

760 Bretherton, C. S., Uttal, T., Fairall, C. W., Yuter, S., Weller, R., Baumgardner, D., Comstock, K., and Wood, R.: The EPIC  
761 2001 stratocumulus study, 2004.

762 Brunner, L., Pendergrass, A. G., Lehner, F., Merrifield, A. L., Lorenz, R., and Knutti, R.: Reduced global warming from  
763 CMIP6 projections when weighting models by performance and independence, *Earth Syst. Dynam.*, 11, 995-1012,  
764 10.5194/esd-11-995-2020, 2020.

765 Buonomo, E., Savage, N., Dong, G., Becker, B., Jones, R. G., Tian, Z., and Sun, L.: Tropical cyclone changes in convection-  
766 permitting regional climate projections: A study over the Shanghai region, *Journal of Geophysical Research: Atmospheres*,  
767 129, e2023JD038508, 2024.

768 CCRS: Singapore’s Third National Climate Change Study (V3): Climate Change Projections to 2100 — Science (Technical)  
769 Report, [https://www.mss-int.sg/docs/default-source/v3\\_reports/v3\\_science\\_report/v3-science-report-full.pdf](https://www.mss-int.sg/docs/default-source/v3_reports/v3_science_report/v3-science-report-full.pdf), 2024.

770 Chapman, S., Syktus, J., Trancoso, R., Thatcher, M., Toombs, N., Wong, K. K.-H., and Takbash, A.: Evaluation of  
771 Dynamically Downscaled CMIP6-CCAM Models Over Australia, *Earth's Future*, 11, e2023EF003548,  
772 <https://doi.org/10.1029/2023EF003548>, 2023.

773 Clark, D., Mercado, L., Sitch, S., Jones, C., Gedney, N., Best, M., Pryor, M., Rooney, G., Essery, R., and Blyth, E.: The Joint  
774 UK Land Environment Simulator (JULES), model description–Part 2: carbon fluxes and vegetation dynamics, *Geoscientific*  
775 *Model Development*, 4, 701-722, 2011.



- 776 Contractor, S., Donat, M. G., Alexander, L. V., Ziese, M., Meyer-Christoffer, A., Schneider, U., Rustemeier, E., Becker, A.,  
777 Durre, I., and Vose, R. S.: Rainfall Estimates on a Gridded Network (REGEN) – a global land-based gridded dataset of daily  
778 precipitation from 1950 to 2016, *Hydrol. Earth Syst. Sci.*, 24, 919-943, <https://doi.org/10.5194/hess-24-919-2020>, 2020.
- 779 Coppola, E., Stocchi, P., Pichelli, E., Torres Alavez, J. A., Glazer, R., Giuliani, G., Di Sante, F., Nogherotto, R., and Giorgi,  
780 F.: Non-Hydrostatic RegCM4 (RegCM4-NH): model description and case studies over multiple domains, *Geosci. Model Dev.*,  
781 14, 7705-7723, 10.5194/gmd-14-7705-2021, 2021.
- 782 CORDEX: CORDEX experiment design for dynamical downscaling of CMIP6, [https://cordex.org/wp-](https://cordex.org/wp-content/uploads/2021/05/CORDEX-CMIP6_exp_design_RCM.pdf)  
783 [content/uploads/2021/05/CORDEX-CMIP6\\_exp\\_design\\_RCM.pdf](https://cordex.org/wp-content/uploads/2021/05/CORDEX-CMIP6_exp_design_RCM.pdf), 2021.
- 784 Cruz, F. T., Narisma, G. T., Dado, J. B., Singhruck, P., Tangang, F., Linarka, U. A., Wati, T., Juneng, L., Phan-Van, T., Ngo-  
785 Duc, T., Santisirisomboon, J., Gunawan, D., and Aldrian, E.: Sensitivity of temperature to physical parameterization schemes  
786 of RegCM4 over the CORDEX-Southeast Asia region, *International Journal of Climatology*, 37, 5139-5153,  
787 <https://doi.org/10.1002/joc.5151>, 2017.
- 788 Desmet, Q. and Ngo-Duc, T.: A novel method for ranking CMIP6 global climate models over the southeast Asian region,  
789 *International Journal of Climatology*, 42, 97-117, <https://doi.org/10.1002/joc.7234>, 2022.
- 790 Di Virgilio, G., Ji, F., Tam, E., Nishant, N., Evans, J. P., Thomas, C., Riley, M. L., Beyer, K., Grose, M. R., Narsey, S., and  
791 Delage, F.: Selecting CMIP6 GCMs for CORDEX Dynamical Downscaling: Model Performance, Independence, and Climate  
792 Change Signals, *Earth's Future*, 10, e2021EF002625, <https://doi.org/10.1029/2021EF002625>, 2022.
- 793 Di Virgilio, G., Evans, J. P., Ji, F., Tam, E., Kala, J., Andrys, J., Thomas, C., Choudhury, D., Rocha, C., White, S., Li, Y., El  
794 Rafei, M., Goyal, R., Riley, M. L., and Lingala, J.: Design, evaluation, and future projections of the NARcliM2.0 CORDEX-  
795 CMIP6 Australasia regional climate ensemble, *Geosci. Model Dev.*, 18, 671-702, 10.5194/gmd-18-671-2025, 2025.
- 796 Doblas-Reyes, F. J., Sörensson, A. A., Almazroui, M., Dosio, A., Gutowski, W. J., Haarsma, R., Hamdi, R., Hewitson, B.,  
797 Kwon, W. T., Lamptey, B. L., Maraun, D., Stephenson, T. S., Takayabu, I., Terray, L., Turner, A., and Zuo, Z.: Linking Global  
798 to Regional Climate Change, in: *Climate Change 2021: The Physical Science Basis. Contribution of Working Group I to the*  
799 *Sixth Assessment Report of the Intergovernmental Panel on Climate Change*, edited by: Masson-Delmotte, V., Zhai, P., Pirani,  
800 A., Connors, S. L., Péan, C., Berger, S., Caud, N., Chen, Y., Goldfarb, L., Gomis, M. I., Huang, M., Leitzell, K., Lonnoy, E.,  
801 Matthews, J. B. R., Maycock, T. K., Waterfield, T., Yelekçi, O., Yu, R., and Zhou, B., Cambridge University Press, Cambridge,  
802 United Kingdom and New York, NY, USA, 1363–1512, <https://doi.org/10.1017/9781009157896.012>, 2021.
- 803 Dosio, A., Panitz, H.-J., Schubert-Frisius, M., and Lüthi, D.: Dynamical downscaling of CMIP5 global circulation models over  
804 CORDEX-Africa with COSMO-CLM: evaluation over the present climate and analysis of the added value, *Climate Dynamics*,  
805 44, 2637-2661, 10.1007/s00382-014-2262-x, 2015.
- 806 Douville, H., Raghavan, K., Renwick, J., Allan, R. P., Arias, P. A., Barlow, M., Cerezo-Mota, R., Cherchi, A., Gan, T. Y.,  
807 Gergis, J., Jiang, D., Khan, A., Pokam Mba, W., Rosenfeld, D., Tierney, J., and Zolina, O.: Water Cycle Changes, in: *Climate*  
808 *Change 2021: The Physical Science Basis. Contribution of Working Group I to the Sixth Assessment Report of the*  
809 *Intergovernmental Panel on Climate Change*, edited by: Masson-Delmotte, V., Zhai, P., Pirani, A., Connors, S. L., Péan, C.,  
810 Berger, S., Caud, N., Chen, Y., Goldfarb, L., Gomis, M. I., Huang, M., Leitzell, K., Lonnoy, E., Matthews, J. B. R., Maycock,  
811 T. K., Waterfield, T., Yelekçi, O., Yu, R., and Zhou, B., Cambridge University Press, Cambridge, United Kingdom and New  
812 York, NY, USA, 1055–1210, <https://doi.org/10.1017/9781009157896.010>, 2021.



- 813 Evans, J. P., Di Virgilio, G., Hirsch, A. L., Hoffmann, P., Remedio, A. R., Ji, F., Rockel, B., and Coppola, E.: The CORDEX-  
814 Australasia ensemble: evaluation and future projections, *Climate Dynamics*, 57, 1385-1401, 10.1007/s00382-020-05459-0,  
815 2021.
- 816 Freidenreich, S. and Ramaswamy, V.: A new multiple-band solar radiative parameterization for general circulation models,  
817 *Journal of Geophysical Research: Atmospheres*, 104, 31389-31409, 1999.
- 818 Funk, C., Peterson, P., Landsfeld, M., Pedreros, D., Verdin, J., Shukla, S., Husak, G., Rowland, J., Harrison, L., Hoell, A., and  
819 Michaelsen, J.: The climate hazards infrared precipitation with stations—a new environmental record for monitoring extremes,  
820 *Scientific Data*, 2, 150066, <https://doi.org/10.1038/sdata.2015.66>, 2015.
- 821 Gibson, P. B., Rampal, N., Dean, S. M., and Morgenstern, O.: Storylines for Future Projections of Precipitation Over New  
822 Zealand in CMIP6 Models, *Journal of Geophysical Research: Atmospheres*, 129, e2023JD039664,  
823 <https://doi.org/10.1029/2023JD039664>, 2024.
- 824 Giorgi, F. and Gutowski, W. J.: Coordinated Experiments for Projections of Regional Climate Change, *Current Climate  
825 Change Reports*, 2, 202-210, <https://doi.org/10.1007/s40641-016-0046-6>, 2016.
- 826 Giorgi, F., Jones, C., and Asrar, G.: Addressing climate information needs at the regional level: The CORDEX framework,  
827 *WMO Bull*, 53, 2008.
- 828 Giorgi, F., Coppola, E., Teichmann, C., and Jacob, D.: Editorial for the CORDEX-CORE Experiment I Special Issue, *Climate  
829 Dynamics*, 57, 1265-1268, <https://doi.org/10.1007/s00382-021-05902-w>, 2021.
- 830 Giorgi, F., Coppola, E., Giuliani, G., Ciarlo, J. M., Pichelli, E., Nogherotto, R., Raffaele, F., Malguzzi, P., Davolio, S., Stocchi,  
831 P., and Drofa, O.: The Fifth Generation Regional Climate Modeling System, RegCM5: Description and Illustrative Examples  
832 at Parameterized Convection and Convection-Permitting Resolutions, *Journal of Geophysical Research: Atmospheres*, 128,  
833 e2022JD038199, <https://doi.org/10.1029/2022JD038199>, 2023.
- 834 Gregory, D. and Rowntree, P.: A mass flux convection scheme with representation of cloud ensemble characteristics and  
835 stability-dependent closure, *Monthly Weather Review*, 118, 1483-1506, 1990.
- 836 Grose, M. R., Narsey, S., Trancoso, R., Mackallah, C., Delage, F., Dowdy, A., Di Virgilio, G., Watterson, I., Dobrohotoff, P.,  
837 Rashid, H. A., Rauniyar, S., Henley, B., Thatcher, M., Syktus, J., Abramowitz, G., Evans, J. P., Su, C.-H., and Takbash, A.: A  
838 CMIP6-based multi-model downscaling ensemble to underpin climate change services in Australia, *Climate Services*, 30,  
839 100368, <https://doi.org/10.1016/j.cliser.2023.100368>, 2023.
- 840 Harris, I., Osborn, T. J., Jones, P., and Lister, D.: Version 4 of the CRU TS monthly high-resolution gridded multivariate  
841 climate dataset, *Scientific Data*, 7, 109, 10.1038/s41597-020-0453-3, 2020.
- 842 Hersbach, H., Bell, B., Berrisford, P., Hirahara, S., Horányi, A., Muñoz-Sabater, J., Nicolas, J., Peubey, C., Radu, R., Schepers,  
843 D., Simmons, A., Soci, C., Abdalla, S., Abellan, X., Balsamo, G., Bechtold, P., Biavati, G., Bidlot, J., Bonavita, M., De Chiara,  
844 G., Dahlgren, P., Dee, D., Diamantakis, M., Dragani, R., Flemming, J., Forbes, R., Fuentes, M., Geer, A., Haimberger, L.,  
845 Healy, S., Hogan, R. J., Hólm, E., Janisková, M., Keeley, S., Laloyaux, P., Lopez, P., Lupu, C., Radnoti, G., de Rosnay, P.,  
846 Rozum, I., Vamborg, F., Villaume, S., and Thépaut, J.-N.: The ERA5 global reanalysis, *Quarterly Journal of the Royal  
847 Meteorological Society*, 146, 1999-2049, <https://doi.org/10.1002/qj.3803>, 2020.



- 848 Hoffmann, P., Katzfey, J. J., McGregor, J. L., and Thatcher, M.: Bias and variance correction of sea surface temperatures used  
849 for dynamical downscaling, *Journal of Geophysical Research: Atmospheres*, 121, 12,877-812,890,  
850 <https://doi.org/10.1002/2016JD025383>, 2016.
- 851 Hurley, P.: Modelling Mean and Turbulence Fields in the Dry Convective Boundary Layer with the Eddy-Diffusivity/Mass-  
852 Flux Approach, *Boundary-Layer Meteorology*, 125, 525-536, 10.1007/s10546-007-9203-8, 2007.
- 853 Hussain, M. and Mahmud, I.: pyMannKendall: a python package for non parametric Mann Kendall family of trend tests,  
854 *Journal of open source software*, 4, 1556, 2019.
- 855 IPCC: Climate Change 2021: The Physical Science Basis. Contribution of Working Group I to the Sixth Assessment Report  
856 of the Intergovernmental Panel on Climate Change, Cambridge University Press, Cambridge, United Kingdom and New York,  
857 NY, USA, 10.1017/9781009157896, 2021.
- 858 IPCC: Climate Change 2022: Impacts, Adaptation and Vulnerability Working Group II Contribution to the Sixth Assessment  
859 Report of the Intergovernmental Panel on Climate Change, Cambridge University Press, Cambridge University Press,  
860 Cambridge, UK and New York, NY, USA, 3056 pp., 10.1017/9781009325844., 2022.
- 861 Ispording, R. N., Alexander, L. V., Bador, M., Green, D., Evans, J. P., and Wales, S.: A Standardized Benchmarking  
862 Framework to Assess Downscaled Precipitation Simulations, *Journal of Climate*, 37, 1089-1110, [https://doi.org/10.1175/JCLI-  
863 D-23-0317.1](https://doi.org/10.1175/JCLI-D-23-0317.1), 2024.
- 864 Jiang, X., Howard, E., Su, C.-H., Ispording, R. N., Ng, B., Chapman, S., Ji, F., Grose, M., Syktus, J., Trancoso, R., Thatcher,  
865 M., Narsey, S., Di Virgilio, G., and Kala, J.: Towards benchmarking the dynamically downscaled CMIP6 CORDEX-  
866 Australasia ensemble over Australia, *Journal of Southern Hemisphere Earth Systems Science*, 75, 10.1071/es24050, 2025.
- 867 Juneng, L., Tangang, F., Chung, J. X., Ngai, S. T., Teh, T. W., Narisma, G., Cruz, F., Phan-Van, T., Ngo-Duc, T.,  
868 Santisirisomboon, J., Singhruck, P., Gunawan, D., and Aldrian, E.: Sensitivity of Southeast Asia rainfall simulations to  
869 cumulus and air–sea flux parameterizations in RegCM4, *Climate Research*, 69, <https://doi.org/10.3354/cr01386>, 2016.
- 870 Kain, J. S.: The Kain–Fritsch Convective Parameterization: An Update, *Journal of Applied Meteorology*, 43, 170-181,  
871 [https://doi.org/10.1175/1520-0450\(2004\)043<0170:TKCPAU>2.0.CO;2](https://doi.org/10.1175/1520-0450(2004)043<0170:TKCPAU>2.0.CO;2), 2004.
- 872 Katzfey, J., Nguyen, K., McGregor, J., Hoffmann, P., Ramasamy, S., Nguyen, H. V., Khiem, M. V., Nguyen, T. V., Truong,  
873 K. B., and Vu, T. V.: High-resolution simulations for Vietnam-methodology and evaluation of current climate, *Asia-Pacific  
874 Journal of Atmospheric Sciences*, 52, 91-106, 2016.
- 875 Kiehl, J. T., Hack, J. J., Bonan, G. B., Boville, B. A., Williamson, D. L., and Rasch, P. J.: The National Center for Atmospheric  
876 Research Community Climate Model: CCM3, *Journal of Climate*, 11, 1131-1149, [https://doi.org/10.1175/1520-  
877 0442\(1998\)011<1131:TNCFAR>2.0.CO;2](https://doi.org/10.1175/1520-0442(1998)011<1131:TNCFAR>2.0.CO;2), 1998.
- 878 Kotlarski, S., Keuler, K., Christensen, O. B., Colette, A., Déqué, M., Gobiet, A., Goergen, K., Jacob, D., Lüthi, D., van  
879 Meijgaard, E., Nikulin, G., Schär, C., Teichmann, C., Vautard, R., Warrach-Sagi, K., and Wulfmeyer, V.: Regional climate  
880 modeling on European scales: a joint standard evaluation of the EURO-CORDEX RCM ensemble, *Geosci. Model Dev.*, 7,  
881 1297-1333, 10.5194/gmd-7-1297-2014, 2014.



- 882 Kowalczyk, E., Wang, Y., Law, R., Davies, H., McGregor, J., and Abramowitz, G.: The CSIRO Atmosphere Biosphere Land  
883 Exchange (CABLE) model for use in climate models and as an offline model, 1615, 2006.
- 884 Lawrence, D. M., Fisher, R. A., Koven, C. D., Oleson, K. W., Swenson, S. C., Bonan, G., Collier, N., Ghimire, B., van  
885 Kampenhout, L., Kennedy, D., Kluzek, E., Lawrence, P. J., Li, F., Li, H., Lombardozzi, D., Riley, W. J., Sacks, W. J., Shi,  
886 M., Vertenstein, M., Wieder, W. R., Xu, C., Ali, A. A., Badger, A. M., Bisht, G., van den Broeke, M., Brunke, M. A., Burns,  
887 S. P., Buzan, J., Clark, M., Craig, A., Dahlin, K., Drewniak, B., Fisher, J. B., Flanner, M., Fox, A. M., Gentine, P., Hoffman,  
888 F., Keppel-Aleks, G., Knox, R., Kumar, S., Lenaerts, J., Leung, L. R., Lipscomb, W. H., Lu, Y., Pandey, A., Pelletier, J. D.,  
889 Perket, J., Randerson, J. T., Ricciuto, D. M., Sanderson, B. M., Slater, A., Subin, Z. M., Tang, J., Thomas, R. Q., Val Martin,  
890 M., and Zeng, X.: The Community Land Model Version 5: Description of New Features, Benchmarking, and Impact of Forcing  
891 Uncertainty, *Journal of Advances in Modeling Earth Systems*, 11, 4245-4287, <https://doi.org/10.1029/2018MS001583>, 2019.
- 892 Maraun, D. and Widmann, M.: Cross-validation of bias-corrected climate simulations is misleading, *Hydrol. Earth Syst. Sci.*,  
893 22, 4867-4873, 10.5194/hess-22-4867-2018, 2018.
- 894 McGregor, J. L.: Economical determination of departure points for semi-Lagrangian models, *Monthly Weather Review*, 121,  
895 221-230, 1993.
- 896 McGregor, J. L.: A new convection scheme using a simple closure, *Current issues in the parameterization of convection*,  
897 BMRC, Melbourne, Australia, Research Report, 93, 33-36, 2003.
- 898 McGregor, J. L.: C-CAM: Geometric aspects and dynamical formulation, CSIRO Atmospheric Research Dickson ACT,  
899 Australia 2005.
- 900 McGregor, J. L.: Recent developments in variable-resolution global climate modelling, *Climatic Change*, 129, 369-380, 2015.
- 901 McGregor, J. L. and Dix, M. R.: An updated description of the conformal-cubic atmospheric model, in: *High resolution  
902 numerical modelling of the atmosphere and ocean*, Springer, 51-75, 2008.
- 903 Ngo-Duc, T., Tangang, F. T., Santisirisomboon, J., Cruz, F., Trinh-Tuan, L., Nguyen-Xuan, T., Phan-Van, T., Juneng, L.,  
904 Narisma, G., Singhruck, P., Gunawan, D., and Aldrian, E.: Performance evaluation of RegCM4 in simulating extreme rainfall  
905 and temperature indices over the CORDEX-Southeast Asia region, *International Journal of Climatology*, 37, 1634-1647,  
906 <https://doi.org/10.1002/joc.4803>, 2017.
- 907 Ngo-Duc, T., Nguyen-Duy, T., Desmet, Q., Trinh-Tuan, L., Ramu, L., Cruz, F., Dado, J. M., Chung, J. X., Phan-Van, T.,  
908 Pham-Thanh, H., Truong-Ba, K., Tangang, F. T., Juneng, L., Santisirisomboon, J., Srisawadwong, R., Permana, D., Linarka,  
909 U. A., and Gunawan, D.: Performance ranking of multiple CORDEX-SEA sensitivity experiments: towards an optimum choice  
910 of physical schemes for RegCM over Southeast Asia, *Climate Dynamics*, 62, 8659-8673, 10.1007/s00382-024-07353-5, 2024.
- 911 Nguyen, K. C., Katzfey, J. J., and McGregor, J. L.: Global 60 km simulations with CCAM: evaluation over the tropics, *Climate  
912 dynamics*, 39, 637-654, 2012.
- 913 Nguyen, P.-L., Bador, M., Alexander, L. V., and Lane, T. P.: Selecting regional climate models based on their skill could give  
914 more credible precipitation projections over the complex Southeast Asia region, *Climate Dynamics*, 61, 3431-3452,  
915 10.1007/s00382-023-06751-5, 2023.



- 916 Nguyen, P.-L., Bador, M., Alexander, L. V., Lane, T. P., and Funk, C. C.: On the Robustness of Annual Daily Precipitation  
917 Maxima Estimates Over Monsoon Asia, *Frontiers in Climate*, 2, <https://doi.org/10.3389/fclim.2020.578785>, 2020.
- 918 Nguyen, P.-L., Bador, M., Alexander, L. V., Lane, T. P., and Ngo-Duc, T.: More intense daily precipitation in CORDEX-SEA  
919 regional climate models than their forcing global climate models over Southeast Asia, *International Journal of Climatology*,  
920 n/a, <https://doi.org/10.1002/joc.7619>, 2022.
- 921 Nguyen, P. L., Alexander, L. V., Thatcher, M. J., Truong, S. C. H., Isphording, R. N., and McGregor, J. L.: Selecting CMIP6  
922 global climate models (GCMs) for Coordinated Regional Climate Downscaling Experiment (CORDEX) dynamical  
923 downscaling over Southeast Asia using a standardised benchmarking framework, *Geosci. Model Dev.*, 17, 7285-7315,  
924 10.5194/gmd-17-7285-2024, 2024.
- 925 O'Neill, B. C., Tebaldi, C., van Vuuren, D. P., Eyring, V., Friedlingstein, P., Hurtt, G., Knutti, R., Kriegler, E., Lamarque, J.  
926 F., Lowe, J., Meehl, G. A., Moss, R., Riahi, K., and Sanderson, B. M.: The Scenario Model Intercomparison Project  
927 (ScenarioMIP) for CMIP6, *Geosci. Model Dev.*, 9, 3461-3482, 10.5194/gmd-9-3461-2016, 2016.
- 928 Pal, J. S., Small, E. E., and Eltahir, E. A. B.: Simulation of regional-scale water and energy budgets: Representation of subgrid  
929 cloud and precipitation processes within RegCM, *J. Geophys. Res.*, 105, 29 579-529 594, 2000.
- 930 Rohde, R. A. and Hausfather, Z.: The Berkeley Earth Land/Ocean Temperature Record, *Earth Syst. Sci. Data*, 12, 3469-3479,  
931 10.5194/essd-12-3469-2020, 2020.
- 932 Rotstayn, L. D.: A physically based scheme for the treatment of stratiform clouds and precipitation in large-scale models. I:  
933 Description and evaluation of the microphysical processes, *Quarterly Journal of the Royal Meteorological Society*, 123, 1227-  
934 1282, 1997.
- 935 Schroeter, B. J. E., Ng, B., Takbashi, A., Rafter, T., and Thatcher, M.: A Comprehensive Evaluation of Mean and Extreme  
936 Climate for the Conformal Cubic Atmospheric Model (CCAM), *Journal of Applied Meteorology and Climatology*, 63, 997-  
937 1018, <https://doi.org/10.1175/JAMC-D-24-0004.1>, 2024.
- 938 Schwarzkopf, M. D. and Ramaswamy, V.: Radiative effects of CH<sub>4</sub>, N<sub>2</sub>O, halocarbons and the foreign-broadened H<sub>2</sub>O  
939 continuum: A GCM experiment, *Journal of Geophysical Research: Atmospheres*, 104, 9467-9488, 1999.
- 940 Sen, P. K.: Estimates of the regression coefficient based on Kendall's tau, *Journal of the American statistical association*, 63,  
941 1379-1389, 1968.
- 942 Seneviratne, S. I., Zhang, X., Adnan, M., Badi, W., Dereczynski, C., Di Luca, A., Ghosh, S., Iskandar, I., Kossin, J., Lewis,  
943 S., Otto, F., Pinto, I., Satoh, M., Vicente-Serrano, S. M., Wehner, M., and Zhou, B.: Weather and Climate Extreme Events in  
944 a Changing Climate, in: *Climate Change 2021: The Physical Science Basis. Contribution of Working Group I to the Sixth  
945 Assessment Report of the Intergovernmental Panel on Climate Change*, edited by: Masson-Delmotte, V., Zhai, P., Pirani, A.,  
946 Connors, S. L., Péan, C., Berger, S., Caud, N., Chen, Y., Goldfarb, L., Gomis, M. I., Huang, M., Leitzell, K., Lonnoy, E.,  
947 Matthews, J. B. R., Maycock, T. K., Waterfield, T., Yelekçi, O., Yu, R., and Zhou, B., Cambridge University Press, Cambridge,  
948 United Kingdom and New York, NY, USA, 1513–1766, <https://doi.org/10.1017/9781009157896.013>, 2021.
- 949 Sobolowski, S., Somot, S., Fernandez, J., Evin, G., Brands, S., Maraun, D., Kotlarski, S., Jury, M., Benestad, R. E., Teichmann,  
950 C., Christensen, O. B., Bülow, K., Buonomo, E., Katragkou, E., Steger, C., Sørland, S., Nikulin, G., McSweeney, C., Döbler,  
951 A., Palmer, T., Wilcke, R., Boé, J., Brunner, L., Ribes, A., Qasmi, S., Nabat, P., Sevault, F., and Oudar, T.: GCM Selection



- 952 and Ensemble Design: Best Practices and Recommendations from the EURO-CORDEX Community, *Bulletin of the American*  
953 *Meteorological Society*, 106, E1834-E1850, <https://doi.org/10.1175/BAMS-D-23-0189.1>, 2025.
- 954 Stevens, B., Fiedler, S., Kinne, S., Peters, K., Rast, S., Müsse, J., Smith, S. J., and Mauritsen, T.: MACv2-SP: A  
955 parameterization of anthropogenic aerosol optical properties and an associated Twomey effect for use in CMIP6, *Geoscientific*  
956 *Model Development*, 10, 433-452, 2017.
- 957 Tangang, F., Chung, J. X., Juneng, L., Supari, Salimun, E., Ngai, S. T., Jamaluddin, A. F., Mohd, M. S. F., Cruz, F., Narisma,  
958 G., Santisirisomboon, J., Ngo-Duc, T., Van Tan, P., Singhruck, P., Gunawan, D., Aldrian, E., Sopaheluwakan, A., Grigory,  
959 N., Remedio, A. R. C., Sein, D. V., Hein-Griggs, D., McGregor, J. L., Yang, H., Sasaki, H., and Kumar, P.: Projected future  
960 changes in rainfall in Southeast Asia based on CORDEX-SEA multi-model simulations, *Climate Dynamics*, 55, 1247-1267,  
961 <https://doi.org/10.1007/s00382-020-05322-2>, 2020.
- 962 Thatcher, M. and McGregor, J. L.: Using a Scale-Selective Filter for Dynamical Downscaling with the Conformal Cubic  
963 Atmospheric Model, *Monthly Weather Review*, 137, 1742-1752, <https://doi.org/10.1175/2008MWR2599.1>, 2009.
- 964 Theil, H.: A rank-invariant method of linear and polynomial regression analysis, *Indagationes mathematicae*, 12, 173, 1950.
- 965 Tiedtke, M.: A Comprehensive Mass Flux Scheme for Cumulus Parameterization in Large-Scale Models, *Monthly Weather*  
966 *Review*, 117, 1779, [https://doi.org/10.1175/1520-0493\(1989\)117<1779:Acmfsf>2.0.Co;2](https://doi.org/10.1175/1520-0493(1989)117<1779:Acmfsf>2.0.Co;2), 1989.
- 967 Truong, S. and Thatcher, M.: Evaluation of clouds in the conformal cubic atmospheric model using the CFMIP observation  
968 simulator package, *International Journal of Climatology*, 45, e8846, 2025.
- 969 Truong, S. C., Ramsay, H. A., Rafter, T., and Thatcher, M. J.: Simulation of an intense tropical cyclone in the conformal cubic  
970 atmospheric model and its sensitivity to horizontal resolution, *Weather and Climate Extremes*, 47, 100744, 2025.
- 971 Truong, S. C. H., Thatcher, M. J., Nguyen, P. L., Alexander, L. V., and McGregor, J. L.: Spectral Nudging Impacts on  
972 Precipitation Downscaling in the Conformal Cubic Atmospheric Model, version CCAM-2504: Insights from Summer 2011,  
973 *EGUsphere*, 2026, 1-31, 10.5194/egusphere-2025-5847, 2026.
- 974 Tucker, S. O., Kendon, E. J., Bellouin, N., Buonomo, E., Johnson, B., and Murphy, J. M.: Evaluation of a new 12 km regional  
975 perturbed parameter ensemble over Europe, *Climate Dynamics*, 58, 879-903, 2022.
- 976 Van Den Besselaar, E. J. M., Van Der Schrier, G., Cornes, R. C., Iqbal, A. S., and Klein Tank, A. M. G.: SA-OBS: A Daily  
977 Gridded Surface Temperature and Precipitation Dataset for Southeast Asia, *Journal of Climate*, 30, 5151-5165,  
978 <https://doi.org/10.1175/jcli-d-16-0575.1>, 2017.
- 979 Vautard, R., Kadyrov, N., Iles, C., Boberg, F., Buonomo, E., Bülow, K., Coppola, E., Corre, L., van Meijgaard, E.,  
980 Nogherotto, R., Sandstad, M., Schwingshackl, C., Somot, S., Aalbers, E., Christensen, O. B., Ciarlo, J. M., Demory, M.-E.,  
981 Giorgi, F., Jacob, D., Jones, R. G., Keuler, K., Kjellström, E., Lenderink, G., Levavasseur, G., Nikulin, G., Sillmann, J.,  
982 Solidoro, C., Sørland, S. L., Steger, C., Teichmann, C., Warrach-Sagi, K., and Wulfmeyer, V.: Evaluation of the Large EURO-  
983 CORDEX Regional Climate Model Ensemble, *Journal of Geophysical Research: Atmospheres*, 126, e2019JD032344,  
984 <https://doi.org/10.1029/2019JD032344>, 2021.
- 985 Way, R. G., Oliva, F., and Viau, A. E.: Underestimated warming of northern Canada in the Berkeley Earth temperature product,  
986 *International Journal of Climatology*, 37, 1746-1757, <https://doi.org/10.1002/joc.4808>, 2017.



- 987 Wilson, D. R. and Ballard, S. P.: A microphysically based precipitation scheme for the UK Meteorological Office Unified  
988 Model, *Quarterly Journal of the Royal Meteorological Society*, 125, 1607-1636, 1999.
- 989 Yasutomi, N., Hamada, A., and Yatagai, A.: Development of a long-term daily gridded temperature dataset and its application  
990 to rain/snow discrimination of daily precipitation, *Global Environmental Research*, 15, 165-172, 2011.
- 991 Yatagai, A., Kamiguchi, K., Arakawa, O., Hamada, A., Yasutomi, N., and Kitoh, A.: APHRODITE: Constructing a Long-  
992 Term Daily Gridded Precipitation Dataset for Asia Based on a Dense Network of Rain Gauges, *Bulletin of the American  
993 Meteorological Society*, 93, 1401-1415, <https://doi.org/10.1175/BAMS-D-11-00122.1>, 2012.
- 994 Zeng, X., Zhao, M., and Dickinson, R. E.: Intercomparison of Bulk Aerodynamic Algorithms for the Computation of Sea  
995 Surface Fluxes Using TOGA COARE and TAO Data, *Journal of Climate*, 11, 2628-2644, [https://doi.org/10.1175/1520-  
996 0442\(1998\)011<2628:IOBAAF>2.0.CO;2](https://doi.org/10.1175/1520-0442(1998)011<2628:IOBAAF>2.0.CO;2), 1998.
- 997 Ziese, M. R.-S., Armin; Becker, Andreas; Finger, Peter; Rustemeier, Elke; Hänsel, Stephanie; Schneider, Udo: GPCC Full  
998 Data Daily Version 2022 at 1.0°: Daily Land-Surface Precipitation from Rain-Gauges built on GTS-based and Historic Data.,  
999 10.5676/DWD\_GPCC/FD\_D\_V2022\_100, 2022.

1000